Institute of Space and Aeronautical Science, University of Tokyo
Report No. 587, December 1980

Water Vapor Content in the Stratosphere Obtained by a Balloon Observation

By

Fumiho TAKAHASHI

CONTENTS

ACKNOWLEDGEMENTS

PREFACE

Chapter I. GENERAL INTRODUCTION

§ 1. REVIEW OF THE STRATOSPHERIC WATER VAPOR 235
1.1 *Stratospheric Water Vapor—Its Origin* 235
1.2 *Influence upon the Thermal Structure of the Earth's Atmosphere* 236
1.3 *Photochemistry of Water Vapor* 237
1.4 *Dynamical Effects and Transport Phenomena* 239
1.5 *Thermal Excitation of Atmospheric Tides* 240
§ 2. SUMMARY OF THE STRATOSPHERIC WATER VAPOR OBSERVATIONS 240
2.1 *Current Methods for Measuring the Stratospheric Water Vapor Concentration* 240
2.2 *Characteristics of In situ and Remote Measurements* 243
§ 3. DISCUSSION 243

Chapter II. SPECTROSCOPIC MEASUREMENTS OF WATER VAPOR

§ 1. INTRODUCTION 243
§ 2. HIGH RESOLUTION ABSORPTION SPECTRA OF WATER VAPOR IN THE σ-BAND REGION 244
2.1 *Experimental Set-Up* 244
2.2 *High Resolution Absorption Spectrum* 246
2.3 *Comparison of Laboratory Spectrum with Sky Spectrum* 248
2.4 *Discussion* 251
§ 3. MEASUREMENTS OF ABSORPTION CROSS SECTIONS IN THE σ-ABSORPTION BAND OF WATER VAPOR 251
3.1 *Principle of Measurement* 251
3.2 *Experimental Instrumentation and Procedure* 252
3.3 *Results and Discussion* 253

Chapter III. DETERMINATION OF WATER VAPOR CONCENTRATION IN THE ATMOSPHERE AND ITS APPLICATION TO BALLOON OBSERVATION IN THE STRATOSPHERE
§ 1. Principle for Determination of Water Vapor Concentration 258
§ 2. Development and System Design of Measuring Instrument and Techniques 262
2.1 *Absorption Cell and Optical System* 262
2.2 *Interference Filter* 263
2.3 *Electronic Circuitry* 263
2.4 *House Keeping* 267
2.5 *Telemetry* 267
§ 3. Vacuum System 269
§ 4. Laboratory Experiments 269
§ 5. Discussion 270

Chapter IV. BALLOON OBSERVATION IN THE STRATOSPHERE
§ 1. Introduction 271
§ 2. Experimental Procedure before Balloon Launching 271
2.1 *Calibration* 271
2.2 *Evacuation of the Vacuum System* 273
§ 3. Balloon Observation 273
§ 4. Experimental Results and Discussion 276
4.1 *Data Processing* 276
4.2 *Contamination from Balloon and Scientific Gondola* 282
4.3 *Flow Process from Troposphere into Stratosphere* 282
§ 5. Suggestions for Further Experimental Works 282
5.1 *Selection of Water Vapor Absorption Lines* 283
5.2 *Light Source and Detector* 283
5.3 *Further Separation from the Balloon* 283
5.4 *Differential Absorption Technique* 284

Chapter V. GENERAL CONCLUSION
References 285

Acknowledgements

The author would like to express his sincere and hearty thanks to Prof. K. Hirao for his continual guidance and stimulating suggestions during the course of this work.

Sincere thanks are also due to late Prof. T. Tohmatsu, Prof. K. Takayanagi, Prof. T. Itoh, Prof. T. Ogawa and Prof. T. Matsuno for their encouragements and valuable discussions.

The author is also indebted to Drs. T. Mukai, K. Oyama, H. Kubo and O. Ashihara for many fruitful discussions and suggestions.

The author is grateful to Prof. N. Fukushima, Dr. K. Suzuki, Dr. E. Kaneda, Mr. N. Iwagami, Mr. K. Shibasaki, University of Tokyo, and Prof. T. Makino, Dr. H. Yamamoto, Rikkyo University, for their encouragements and valuable advice to the present work.

The author also wishes to express gratitude to Prof. H. Kamiyama, Prof. M. Tanaka, Tohoku University, Prof. M. Hirono, Kyusyu University, Prof. S. Kawaguchi, Prof. H. Fukunishi, National Institute for Polar Research, for their encouragements and valuable discussions.

A part of the experiments reported in this thesis was done by Mr. S. Ishii to fulfill author's investigations. Many helpful suggestions on electronic circuitry were given by Mr. H. Honda.

The author also wishes to express gratitude to Dr. H. Thiemann of the Institut für Physikalische Weltraumforschung, Germany, for his encouragement and critical reading the manuscript.

Many thanks are due to Prof. T. Obayashi, Prof. A. Nishida, Prof. Y. Nakamura, Dr. T. Terasawa, Mr. S. Machida, Institute of Space and Aeronautical Science, University of Tokyo.

The balloon launching was successfully carried out under the cooperation of the members of the Space Engineering Division of the I.S.A.S.

Managements of the complicated balloon experiment were done by Prof. J. Nishimura and Prof. H. Hirosawa and others.

The author must express his sincere gratitude to Dr. S. Namba of the Sendai District Meteorological Observatory for his offer of the valuable aerological data.

Finally the author expresses his gratitude to Miss T. Okamoto for her typewriting of this thesis and to Machiko, the author's wife, for her continual encouragement and stimulating discussions.

Preface

Water vapor causes a variety of interesting phenomena in the earth's atmosphere. On the one hand, atmospheric water vapor is, of course, primarily responsible for a number of meteorological phenomena such as cloud or rainfall. In particular in the case of a typhoon or a hurricane, water vapor might become the energy source producing and maintaining such a giant tropical cyclone. On the other hand, it is well known that many optical phenomena exist in the atmosphere. For example, we can often see haloes and coronas in the cirrostratus above 6 km. Since their discovery in 1870, the iridescent "mother-of-pearl" clouds have been extensively observed at altitudes from 17 to 31 km over Norway or Alaska. In the summer of 1885, northern european scientists found the mysterious clouds gleaming in the evening sky, which were later named "noctilucent clouds". These clouds are formed at heights around the mesopause ($\sim$83 km) and they can only be seen in summertime and mainly in the latitude range of 50°N–65°N.

Immense efforts have been done to find out the mechanism of these interesting phenomena, and all these phenomena are now believed to be due to atmospheric

water vapor. Although atmospheric water vapor has been playing many important roles in the various phenomena taking place on the earth, it is considered recently to be the key constituent from the following aspects.

The first aspect is related to heat budget of the earth and the thermal structure of its atmosphere. The solar radiation is strongly absorbed by atmospheric water vapor especially in the long-wave region. This leads to the important problems on the radiation field, radiative albedo, and the energy balance of the earth/atmosphere system. As far as heat is concerned, the so-called "greenhouse" effect due to terrestrial water vapor is larger than any other atmospheric species.

The second aspect is related to the chemistry of H_2O. Water vapor is thought to be the primary source of the hydrogen compounds such as H, H_2, HO_x (OH and HO_2), and so on. Among these species, H and H_2 diffuse upwards and form the geocorona outside the terrestrial atmosphere and this process might account for the sink of atmospheric water vapor and/or the hydrogen compounds. On the other hand, HO_x plays a significant role in the chemistry of the upper atmosphere. In particular in the stratosphere, HO_x not only destroys atmospheric ozone catalytically, but also takes part of a number of chemical or photochemical reactions with NO_x, ClO_x, aerosols, and so on.

The third aspect is related to the thermal excitation of atmospheric tides. Below the thermosphere, atmospheric thermal tides are primarily excited by O_3 and H_2O insolation absorption. In calculating the heating rates which produces atmospheric tides, it is quite natural that the heating rates are directly controlled by the altitude profile of the water vapor density. It is well known that these atmospheric waves propagate upwards and determine the mean winds in the mesosphere and thermosphere.

Since water vapor concentration was first measured by Dobson, Brewer, and Cwilong in 1945, a lot of measurements have been done by means of various methods and techniques. Although the atmosphere of the stratosphere is believed to be quite dry in general, no water vapor measurement are routinely available in the stratosphere, because water vapor concentration is too small to be reliably measured. Most of the past measurements are restricted to the United States and Europe. Further a discrepancy of one order of magnitude has been reported at the height of 25 km between Mastenbrook's and Sissenwine's measurement which were done by the same frost-point hygrometer. We believe that technique to measure stratospheric water vapor is not well established.

This thesis describes a technique which has been newly developed to measure water vapor concentration in the stratosphere. To begin with, we briefly review the effects of atmospheric water vapor in the stratospheric aeronomy in Chapter I. In the same Chapter, we summarize the currently available and widely used techniques to measure the stratospheric water vapor concentration. Finally, main problems and significance of stratospheric water vapor observation will be clarified.

Chapter II describes the results and the experimental instrumentation of laboratory spectroscopic measurements which were done before balloon observation.

Chapter III is devoted to the theoretical investigation on determination of water

vapor concentration in the atmosphere and the system description for its application to balloon observation in the stratosphere. In addition, some results of the laboratory experiments are shown.

In Chapter IV, the practical procedure and experimental results of the balloon observation on the basis of the results of the preceding Chapter are described briefly. After that, the observational results are discussed and compared with available data so far obtained.

Some problems associated with this measuring technique are presented from the various points of view, and suggestions for further observational works are given.

General conclusion is given in Chapter V.

Chapter I. GENERAL INTRODUCTION

§ 1. Review of the Stratospheric Water Vapor

1.1 *Stratospheric Water Vapor—Its Origin*

Brewer (1949) and Dobson (1956) postulated a model of the stratospheric moisture mechanism in which air passes regularly through the tropical tropopause via a meridional circulation. That is, the air ascends in the tropics, is cooled, and is dried out by condensation. This air penetrates the tropical tropopause (at about 100 mb, frequently with temperatures of $-83°C$) and flows polewards. If saturated at the tropical tropopause, stratospheric air moving poleward and descending slightly would arrive over Northern Europe, Greenland, and the Northern USSR with frost points for the extreme dryness of the lower stratosphere (Dobson et al., 1946; Brewer et al., 1948; Hesstvedt, 1959). To complete the circulation, the poleward moving stratospheric air must descend into the troposphere at higher latitudes (Gutnick, 1961; Stanford, 1973).

This is the so-called "Brewer-Dobson circulation". This "Hadley cell" circulation contributes to the natural sources of water vapor injected into the stratosphere. Besides, the following natural sources are generally accepted:

(1) Thunderstorms that penetrate the tropopause,
(2) Exchange of air through tropopause breaks or folds,
(3) Volcanic eruptions, and
(4) Oxidation of natural methane.

Source estimates of the Hadley cell, thunderstorms that penetrate the tropopause, and oxidation of natural methane have been given in the work by Weickmann and Van Valin (1972, 1974).

With respect to exchange of air, the detailed description will be given in Subsection 1.4.

Finally, we briefly review sinks of stratospheric water vapor below. The assessment of sinks of stratospheric water vapor is much more difficult than that of the sources. While there is no question about the existence of tropical upwelling (includ-

ing convective cells) as a regional sources, the descending branch of the classical Hadley cell has never been clearly localized. The polar regions in winter, especially the Antarctic, appear to provide the only strong sink (e.g., Stanford, 1973). The other loss mechanisms for water vapor are absorptions by hygroscopic aerosols, absorption on surfaces of particles (e.g., Carbon), gradual upward diffusion, downward intrusions into the troposphere, and photochemical destruction. However at the present state of knowledge, it is impossible to give further discussions.

1.2 *Influence upon the Thermal Structure of the Earth's Atmosphere*

First, we show the absorption spectra for H_2O, CO_2, O_3, N_2O, CH_4 and the absorption spectrum of the atmosphere in Fig. 1–1. As we can see in this figure, there exist a number of intense water vapor absorption bands in the infrared region. The existence of such a number of strong water vapor absorption bands accounts for the importance of atmospheric water vapor in the radiation, heat, and energy balance of the earth/atmosphere system (see Craig, 1965).

In general heat budget of the earth is controlled by two kinds of radiation, short-wave radiation from the sun and long-wave radiation from the earth itself. However, since the total radiant power by long-wave radiation exceeds greatly that of the solar short-wave radiation, the thermal balance of the earth is, principally, dominated by long-wave radiation.

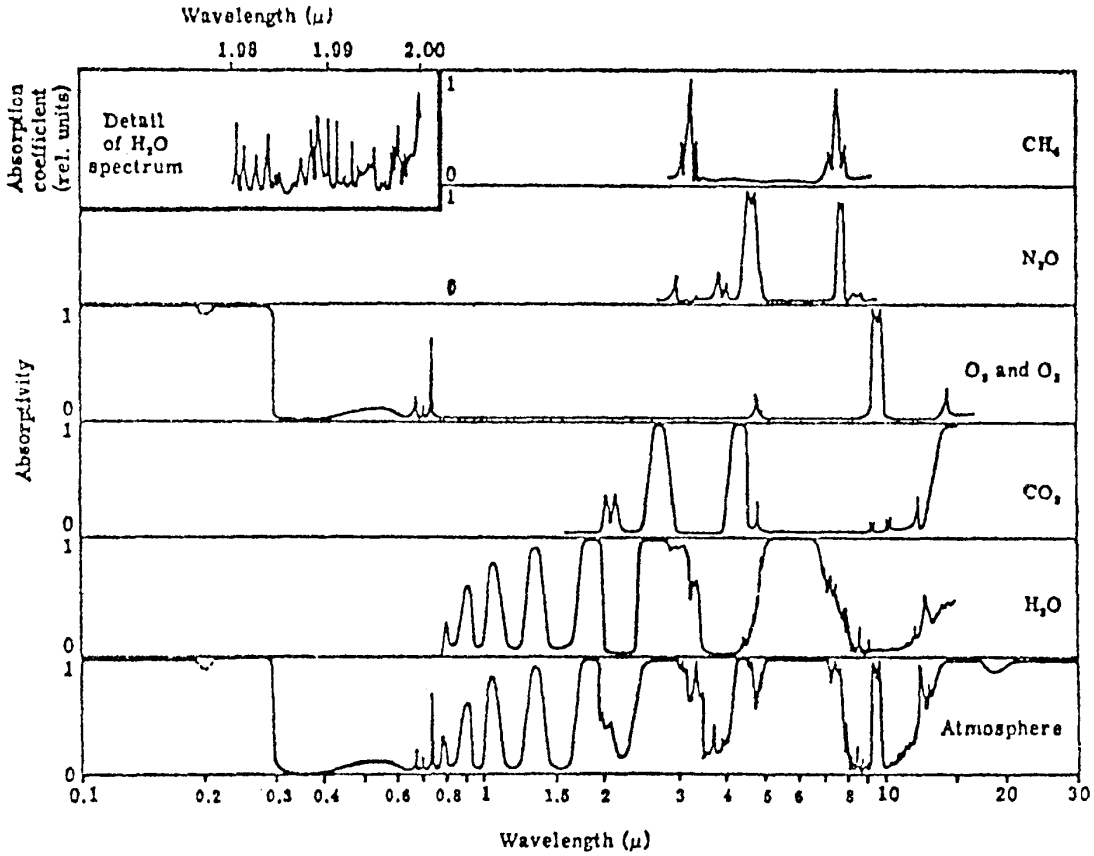

FIG. 1–1. Absorption spectra for H_2O, CO_2, O_3 N_2O, CH_4 and the absorption spectrum of the atmosphere (Howard, 1959; Goody and Robinson, 1951).

As the atmosphere and ground of the earth emit black-body radiation corresponding to the temperature of about 300°K, the wavelength which gives the maximum radiant power occurs in the 5–15 μm region. In this wavelength region, there exists a number of atmospheric absorption bands such as H_2O 6.3 μ, O_3 9.6 μ, and CO_2 15 μ as can be seen in Fig. 1–1. In consequence of long-wave radiation being trapped by the terrestrial atmosphere, the so-called "green house effect" takes place in the earth/atmosphere system. Many workers have examined the "greenhouse effect" due to the various atmospheric molecules (e.g., Manabe and Wetherald, 1967; Kuhn and London, 1969; Shimazaki, 1979). It is noteworthy that the water vapor concentration in the stratosphere is a dominant factor of the "greenhouse effect". That is, if the stratospheric water vapor density increases up to twice of the present value, the surface temperature of the earth might increase by approximately 1°K from the work of Manabe and Wetherald (1967). It is believed that even 1°K surface temperature change causes a drastic change of our atmosphere. Therefore to monitor the water vapor density in the stratosphere is of great importance from the standpoint of the energy budget of the earth/atmosphere system.

1.3 *Photochemistry of Water Vapor*

The classical and pioneering work in this field has been made by Bates and Nicolet (1950) in order to examine the photochemical process of water vapor. In their work, a fundamental concept on the hydrogen-oxygen atmosphere were stated such as the photodissociation of water vapor,

$$H_2O + h\nu(\lambda < 242\ \text{nm}) \rightarrow OH + H, \qquad \text{(R1)}$$

and its reformation processes,

$$H + OH + M \rightarrow H_2O + M \qquad \text{(R2)}$$

$$H + HO_2 \rightarrow H_2O + O \qquad \text{(R3)}$$

$$OH + OH \rightarrow H_2O + O \qquad \text{(R4)}$$

$$OH + HO_2 \rightarrow H_2O + O_2 \qquad \text{(R5)}$$

$$H_2 + O + M \rightarrow H_2O + M \qquad \text{(R6)}$$

$$H_2 + OH \rightarrow H_2O + H, \qquad \text{(R7)}$$

where M denotes the third body concerning each reaction. However because of the lack of the reaction rates, the quantitative discussions on the photochemistry of water vapor could not be made in their paper.

Hunt (1966) extended the argument of the hydrogen-oxygen atmosphere to the photochemistry of ozone in the stratosphere. He pointed out that the dissociation of water vapor by $O(^1D)$,

$$H_2O + O(^1D) \rightarrow 2 \cdot OH, \qquad \text{(R8)}$$

is of great importance at the lower levels as the main source of free hydrogen because of its rapid reaction rate. In the stratosphere this loss mechanism of H_2O is much more significant than that of (R1). Furthermore, the reaction chains,

$$H+O_3 \rightarrow OH+O_2 \qquad (R\ 9)$$

$$OH+O \rightarrow H+O_2 \qquad (R10)$$

$$HO_2+O \rightarrow OH+O_2 \qquad (R11)$$

Net: $$HO_2+2\cdot O+O_3 \rightarrow OH+3\cdot O_2 \qquad (R12)$$

and $$OH+O_3 \rightarrow HO_2+O_2 \qquad (R13)$$

$$HO_2+O_3 \rightarrow OH+2\cdot O_2 \qquad (R14)$$

Net: $$2\cdot O_3 \rightarrow 3\cdot O_2, \qquad (R15)$$

imply that the HO_x destroy the odd oxygen catalytically. The reactions of (R12) and (R15) are the effective some to destroy the stratospheric ozone in the altitude range above 45 km and below 22 km respectively (Shimazaki and Ogawa, 1974). From the aspect of heat budget of the earth's atmosphere, the problem on the ozone destruction by HO_x led to a lot of investigations of the photochemistry of ozone and the other minor constituents in the stratosphere (see, e.g., Nicolet, 1970; Wofsy, 1974; Shimazaki and Ogawa, 1974; CIAP monograph 1; 1975, Liu et al., 1976; Crutzen, 1978).

At present, water vapor chemistry in the stratosphere is believed to be initiated by oxidation of H_2 and CH_4 by $O(^1D)$ besides the reaction (R8),

$$O^1(^1D)+H_2 \rightarrow H+OH \qquad (R16)$$

$$O(^1D)+CH_4 \rightarrow CH_3+OH \qquad (R17)$$

(see, e.g., Wofsy et al., 1972; Liu and Donahue, 1974). Thus the presence of $O(^1D)$ atoms produced by the photolysis of O_2 and O_3 leads to the possibility of the production of hydrogenic compounds such as H, OH, and HO_2 by H_2O, H_2, and CH_4. Among these dissociated species, H as well as H^+ diffuses upwards gradually and one part forms the geocorona outside the terrestrial atmosphere and another part escapes from the terrestrial atmosphere to the interplanetary space (Hunten and Strobel, 1974; Liu and Donahue, 1974). This process might account for the sink of atmospheric water vapor and/or the hydrogen compounds.

On the other hand, OH and HO_2 not only destroy the atmospheric ozone catalytically as stated previously, but also take part of a number of photochemical reactions with NO_x (Nicolet, 1972; Wofsy and McElroy, 1974), ClO_x (Molina and Rowland, 1974, Stolarski and Cicerone, 1974; Ogawa, 1976; Crutzen, 1978), CH_4 and CO (Wofsy et al., 1972), and aerosols (Junge, 1961) (see also CIAP monograph 1, 1975).

A characteristic of the resulting reactive hydrogen chemistry is that H_2O is the ultimate beneficiary of H_2 and CH_4 oxidation through the fast recycling reaction,

$$OH + HO_2 \rightarrow H_2O + O_2, \qquad (R5)$$

where HO_2 is formed in the three-body reaction

$$H + O_2 + M \rightarrow HO_2 + M. \qquad (R18)$$

From the standpoint of water budget in the stratosphere, it is important to note that the water production rate by the following overall methane oxidation process

$$CH_4 + 2 \cdot O_2 \rightarrow 2H_2O + CO_2, \qquad (R19)$$

which is primarily initiated by hydroxyl free radicals, involves a complex set of reactions with formaldehyde and carbon monoxide and intermediates, greatly exceeds the rate of the above-mentioned exospheric escape of hydrogen from the upper atmosphere (Liu and Donahue, 1974). Consequently, the transfer of water from the stratosphere to the troposphere must exceed the transfer of tropospheric water to the stratosphere, which will be discussed in the following Subsection.

Some mechanisms have been so far proposed (Stanford, 1973; Johnston and Solomon, 1979) to solve this problem, however, it remains still unknown at the present stage.

1.4 *Dynamical Effects and Transport Phenomena*

So far, no more plausible explanation has appeared than the original one of Brewer (1949) and Dobson (1956) that all air entering the stratosphere is forced through the cold water vapor trap of the tropical tropopause. To date, no data have been produced to support any other significant mechanism for tropospheric to stratospheric transport of air by natural atmospheric processes. Recently Kida (1977) found that the Lagrangian motion of air parcels in the stratosphere is consistent with the above Brewer-Dobson circulation. In the lower stratosphere, the vertical mixing by eddy diffusion is quite difficult to occur, because the vertical eddy diffusion coefficient of about $10^4\ cm^2 \cdot sec^{-1}$ (see, e.g., McElroy and McConnell, 1971; Crutzen, 1978) corresponds to its characteristic time of 1–2 years. Therefore if the laminar structure of a certain substance is once formed in the lower stratosphere, its structure remains until the atmosphere of the stratosphere is completely exchanged for the tropospheric air.

On the other hand, Ellsaesser (1974) reviewed the literature on the net mass flux of air from troposphere to stratosphere in the tropical Hadley cell and on the mean tropical tropopause temperatures. He stated that there appeared to be a discrepancy in the water budget with respect to the global circulation model and asked, 'How does the stratosphere maintain a mean mixing ratio of around 4 ppmV (Mastenbrook, 1971) when all air entering the stratosphere passes through a cold trap whose characteristic mixing ratio is not less than 5 ppmV saturation at mean tropical tropopause temperature) and when there is presumptive evidence for direct stratospheric injections of additional H_2O via CH_4 oxidation, the subtropical tropopause gaps, and cumulonimbus penetration of the tropopause?'

From these discussions, a certain mechanism to decrease the stratospheric water vapor is required to support the 'dry' stratosphere. Matsuno (1979) concluded that the cyclone plays a significant role in the intrusions of stratospheric air down into the troposphere from the analytical results by Briggs and Roach (1963) and Danielsen (1968). However, because of the accompanying upward intrusion into the stratosphere of an equal mass of presumably moister tropospheric air, we cannot decide whether the net effet is a source or sink for water vapor at the present state of knowledge (see CIAP monograph 3, 1975).

Besides this mechanism, Stanford (1973) suggested an additional sink for stratospheric water to the descending branches of the Hadley cell model of the general circulation as condensation and precipitation during the antarctic winter night. In addition, the gradual diffusion of water vapor upward into the upper atmosphere might be one candidate for the sink.

In fact, even if the mean motion or circulation in the stratosphere is the Brewer-Dobson circulation, we still have a number of unknown problems such as the intrusions of the tropospheric air into the stratosphere or the dynamical processes in the vicinity of the jet stream core associated with the turbulences or waves.

1.5 *Thermal Excitation of Atmospheric Tides*

According to the theory of atmospheric tides (e.g., Siebert, 1961), it became clear that atmospheric thermal tides are primarily excited by O_3 and H_2O insolation absorption below the thermosphere. The amplitude of the heating due to absorption by water vapor is quite small; nevertheless, the heating affects the entire troposphere and is in phase at all levels. In calculating the heating rates which produces atmospheric tides, it is quite natural that the heating rates are directly controlled by the altitude distribution of the water vapor density. It is well known that these atmospheric waves propagate upwards and determine the mean winds in the mesosphere and thermosphere.

§ 2. Summary of the Stratospheric Water Vapor Observations

2.1 *Current Methods for Measuring the Stratospheric Water Vapor Concentration*

This Subsection summarizes the currently available and presently used techniques to measure the stratospheric water vapor in situ or total content within a column above or below the instrument platform. An extensive bibliography is given in an article by Harries (1976).

So far the largest number of measurements have been made by British scientists (Dobson et al., 1946; Gutnick, 1961) and in the United States, extensively by Mastenbrook and Sissenwine (Mastenbrook and Dinger, 1961; Mastenbrook, 1968, 1971, 1974; Sissenwine, 1968) with the frost-point hygrometer. Variants of the instrument, which is an ingenious development of the common dew-point hygrometer for use at

very low temperature, have been described fully by Brewer, Cwilong, and Dobson (1948).

Another in situ device is the Al_2O_3 sensor developed by Panametrics, Inc. In this device, the calibration seems to be unstable at very low temperatures and humidities, further elaborate calibration efforts are needed. Quite recently, the measurement using the sophysticated Al_2O_3 sensor has been made by Chleck (1979).

Observations of water vapor content have also been made by direct sampling (Barclay et al., 1960) and cryogenic sampling (Ehhalt et al., 1975; Heidt, 1978). Air is drawn through a nitrogen- or helium-cooled vapor trap, resulting in the freezing-out and collection of water. The package is recovered and the amounts of collected water are determined by laboratory analysis.

All of recent new in situ techniques utilize the absorption due to water vapor and have the light source in each instrument (Patel et al., 1974; Bertaux and Delannoy, 1978; Takahashi and Hirao, 1979). Patel et al. used a spin-flip Raman laser and Takahashi and Hirao employed a light emitting diode as a light source. Both groups adopted a multipass absorption cell which was opened to the ambient atmosphere. On the other hand, Bertaux and Delannoy used a Lyman-α source and the small chamber for the sensing region, and have measured detailed distribution of water vapor in the 12–25 km altitude region (see Table 1).

Optical methods have been used for many years because water vapor has strong absorption lines in the infrared region. There are two types of instruments, the radio-

TABLE 1. Summary of Stratospheric Water Vapor Observations

1. *In-situ Observations*

Type	Platform	Location	Altitude (km)	Volume Mixing Ratio (ppmV)	Author
Frost-point hygrometer	Balloon	U.S. (39°N)	12–29	4–13.4	Mastenbrook (1974, 1976)
	Balloon	U.S. (40°N)	10–30	3–30	Sissenwine (1968)
Al_2O_3 hygrometer	Balloon	U.S. (38°N)	10–20	1– 3	Chleck (1979)
Cryogenic sampler	Rocket	U.S. (31°N)	43.6–62.3	3–10	Ehhalt et al. (1975)
	Balloon	Canada (52°N)	23–35	4– 6	Heidt (1978)
Gas sampler	Balloon	U.K. (54°N)	27	52	Barklay et al. (1960)
New techniques:	Platform	Location	Altitude (km)	Volume Mixing Ratio (ppmV)	Author
SFR-laser absorption	Balloon	U.S. (32°N)	28	1.5	Patel et al. (1974)
UV-fluorescence	Balloon	France (44°N)	10–24	7–20	Bertaux and Delannoy (1978)
IR-filter absorption	Balloon	Japan (38°N)	18.6–20.2	10–24	Takahashi and Hirao (1979)

TABLE 1. Summary of Stratospheric Water Vapor Observations (continued)

2. *Remote Soundings*

IR technique	Wave-length (μm)	Platform	Location	Altitude (km)	Volume Mixing Ratio (ppm)	Author
Absorption Spectroscopy (Solar Radiation)	6.27	Balloon	France (44°N)	20–37	3.4	Ackermann (1974)
	6.27	Balloon	U.S. (32°N)	25–30	3.5–4.2	Murcray et al. (1969)
	6.27	Balloon	U.S. (32°N)	14–20	2.4	Farmer (1974)
	2.6	Aircraft	North-South U.S. (70°N–40°S)	10.7–18.3	2.4 (65°N) 1.8 (30°S)	Mckinnon and Morewood (1970)
	2.6	Rocket	Australia (31.5°S)	15–45	1	de Jonckheere (1975)
	2.6	Aircraft	U.K. (54°N)	12.2–14.6	2.7–3.8	Houghton and Seeley (1960)
Emission Spectrometer	6.3	Balloon	U.S. (32°N)	12–29	0.6–4.2	Murcray et al. (1973a)
	24–29	Balloon	U.S. (32°N)	9–29	1.7	Goldman et al. (1973a)
Emission Radiometer	5.5–8	Balloon	U.K. (54°N)	0–25	4.2	Williamson and Houghton (1966)
	5– 7	Balloon	U.S. (42°N)	15–25	4.2	Pick and Houghton (1969)
	17–21	Aircraft	U.S. (34–50°N)	12	4–21	Kuhn et al. (1969, 1971)
	19–35	Aircraft	France (44°N)	12–15	3–13	Kuhn et al. (1975, 1976)
	20–50	Balloon	U.S. (34–50°N)	16–37	3– 8	Chaloner (1975)
	20–60	Balloon	Canada (43°N)	12–25	2.8	Brewer and Thomson (1972)
	$\geqq$40	Balloon	Australia (34°S)	10–28	2– 8	Hyson and Platt (1974)
Emission Interfero-meter	300–1000	Aircraft	U.K. (45–64°N) Arctic Circle (72.5°N)	10–15	1.4–4.2	Harries et al. (1973)
	220–2000	Balloon	France (44°N)	16–36	3–4	Harries et al. (1976)

meter and the spectrometer (interference spectrometer), which measure either the emission from atmospheric water vapor or the absorption of solar radiation by water vapor in the 2.6 and 6.3 μm band (Houghton and Seeley, 1960; Williamson and Houghton, 1966; Pick and Houghton, 1969; Murcray et al., 1960, 1969; Mckinnon and Morewood, 1970; Ackermann, 1974; Farmer, 1974; de Jonckheere, 1975) and

the rotation band (Kuhn et al., 1969, 1971; Brewer and Thomson, 1972; Goldman et al., 1973a; Hyson and Platt, 1974; Chaloner, 1975; Kuhn et al., 1975, 1976). The NPL (National Physical Laboratory, England) group has used Fourier transform spectroscopy in the far infrared with a Michelson interferometer (Harries, 1973; Harries et al., 1974).

2.2 *Characteristics of In situ and Remote measurements*

As we have seen in the preceding Subsection, there is a large variety of instruments and techniques which have been used and which are now in use. These instruments and techniques can be classified into two categories. One is in situ observations, and another is remote soundings. In general, there are likely to be less errors involved in such a direct measurement as frost-point hygrometers compared with the more indirect measurement, for example those using spectral techniques. Because in remote measurements to get the water vapor concentration requires the transfer of the measured numbers through several analytical stages, each one possibly involving errors. On the other hand, an in situ measurement is much more vulnerable to contamination problems than remote measurement. Water vapor observations in the stratosphere are summarized in Table 1.

§ 3. Discussion

Water vapor plays significant roles in the earth's atmosphere, as we have already seen in Section 1. In particular in the stratosphere, water vapor is exceedingly important substance from the standpoint of heat budget of the earth/atmosphere system and photochemistry in the stratosphere. Therefore, it is necessary to know the natural background of water vapor in the stratosphere, its latitudinal and temporal variations, its residence time, and its sources and sinks.

Measurements of water vapor in the stratosphere for this purpose are few and mostly restricted to the United States and Europe. As we can see in Table 1, the absolute value of the stratospheric mixing ratio is still in some doubt and in addition may be considerably different for different locations and times. From these results, further observations are highly recommended.

Chapter II. SPECTROSCOPIC MEASUREMENTS OF WATER VAPOR

§ 1. Introduction

Water vapor has intense absorption bands ranging from the visible to the microwave region. These absorption bands are due to the vibrational and/or rotational excitation of water vapor. The vibration-rotation spectra of water vapor are rich and complex because of their large dipole moments and the great difference of the three moments of inertia. Water vapor has three fundamental frequencies for vibra-

tions of XY_2-type molecules, the bending vibration ν_2 having the lowest frequency (1594.78 cm^{-1}) while ν_2 (3657.05 cm^{-1}) and ν_3 (3755.92 cm^{-1}) both are approximately twice this frequency. The close coincidence between ν_1, ν_3, and $2\nu_2$ implies complex interactions between states (see, for example, Herzberg, 1950; Goody, 1964; Kondratyev, 1969). The complicated interaction between states makes the water vapor spectrum so complicated. The comparatively large amount of water vapor in the earth's atmosphere gives observable absorption in the solar spectrum for some very weak transitions (Delbouille and Roland, 1963; Takahashi and Hirao, 1979a). A large number of water vapor bands in the visible spectrum are relatively weak and therefore they can not be used in the present study.

In the near infrared region, there exists a stronger group of water vapor bands, some of which show complete black-out in the solar spectrum as illustrated in Fig. 1–1. They are commonly identified in groups by the Greek letters ρ, σ, τ, ϕ, ψ, and Ω (Goody, 1964). We take the σ-band absorption for our present purpose by the following reasons.

(1) No absorption band of other atmospheric molecules exists in the 0.94 μm spectral region.
(2) This absorption band has comparatively intense rotational lines.
(3) There exists the intense light source (Light-Emitting-Diode, LED) in this spectral region.
(4) The photomultiplier (hereafter referred to as PM) is available as a detector in the σ-band region.

The σ-band absorption is fundamentally caused by the vibrational transtion between (0, 0, 0) ground state and (2, 0, 1) and (3, 0, 0) excited state, where (0, 0, 0) denotes $(\nu_1, \nu_2, \nu_3)=(0, 0, 0)$. Further, as a number of rotational lines are accompanied with this vibration spectrum, its absorption spectrum is quite complicated.

In this Chapter, we describe labolatory measurements of the water vapor σ-band absorption carried out in order to evaluate the feasibility of water vapor observation in the stratosphere.

§ 2. High Resolution Absorption Spectra of Water Vapor in the σ-Band Region

First, high resolution absorption spectra of water vapor are recorded in the spectral region of interest. These spectra might enable us to determine the absorption lines which should be selected to obtain the strongest absorption in this spectral region.

2.1 *Experimental Set-Up*

The block diagram for obtaining a high resolution absorption spectrum is shown in Fig. 2–1. A Light Emitting Diode (hereafter referred to as LED, NEC-SE301A) is used as a source of continuous radiation and its features will be discussed in Subsection

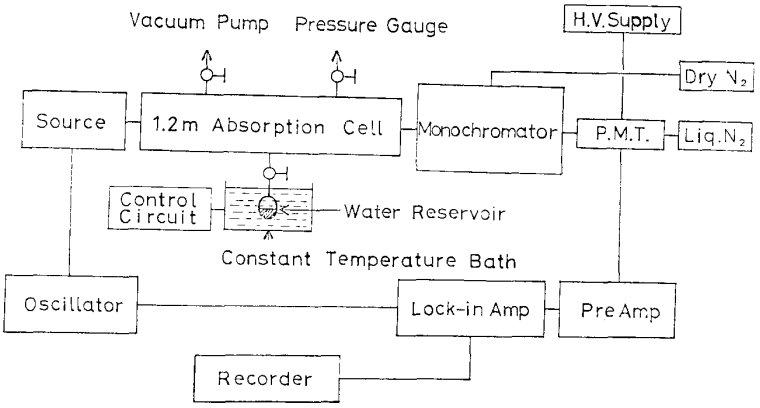

FIG. 2–1. Block diagram for obtaining a high resolution absorption spectrum.

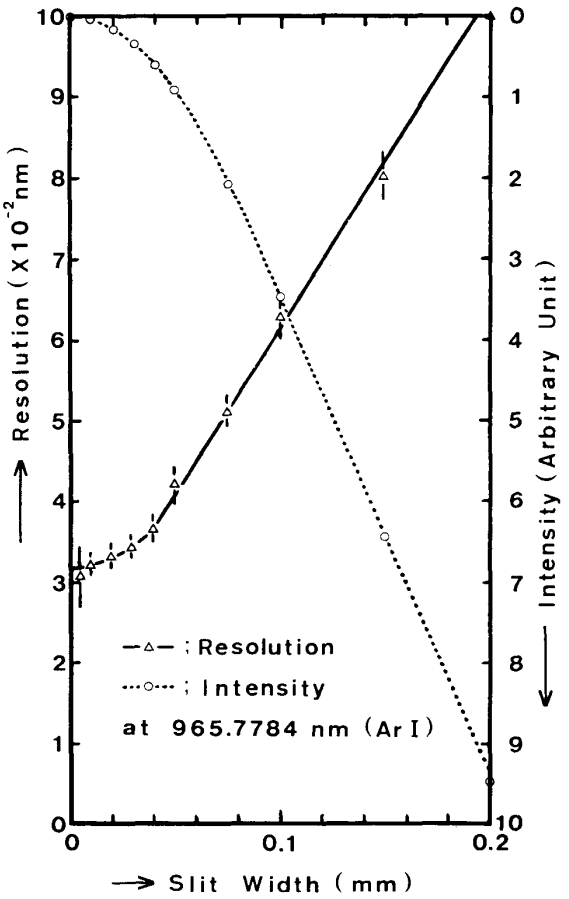

FIG. 2–2. Spectral characteristics of the monochromator used in this experiment.

3.2. To obtain a high resolution spectrum, LED is chopped electrically at 1.2 kHz to improve the S/N ratio as will be stated below. As a grating monochromator for these experiments, we use a Jasco Model CT-80D double monochromator whose spectral chatacteristics are indicated in Fig. 2–2. It should be noted that the nonlinear effect occurs due to a slit width narrower than about 40 μm. A liquid nitrogen cooled

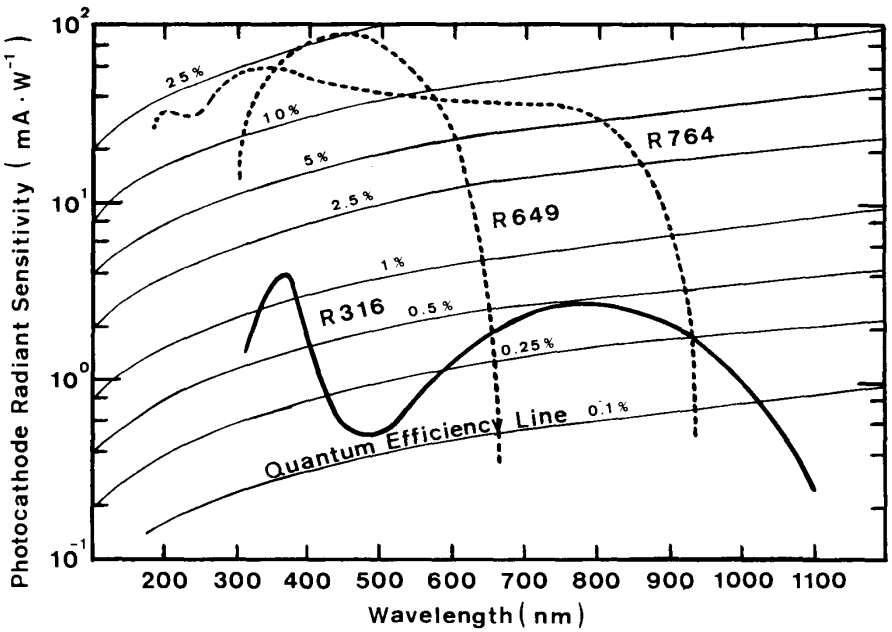

FIG. 2–3. Photocathode radiant sensitivity versus wavelength of HTV-R316 photomultiplier used in this experiment.

PM (HTV-R316) is used as a radiation sensor. The photocathode radiant sensitivity versus wavelength is shown in Fig. 2–3. As we can see in this figure, the quantum efficiency of R316-PM is about 0.23% at 0.94 μm. A high voltage source of -1250 volts is applied. The monochromator is filled with dry nitrogen in order to exclude the contamination by the water vapor in the ambient room atmosphere. To improve the *S/N* ratio, a PAR Model 126 Lock-in Amplifier and a Model 116 Pre-Amplifier is used at a reference frequency of 1.2 kHz. The entrance-exist slit width is approximately 80 μm when the absorption spectrum is taken. The scanning speed of the monochromator adopted is exceedingly slow (0.01 nm$\cdot$min^{-1}) because of the low-pass filter with extraordinarily long time constant (100 seconds). Therefore, it takes about 6 hours to scan the wavelength from 941 nm to 945 nm.

2.2 *High Resolution Absorption Spectrum*

In Fig. 2–4, a high resolution absorption spectrum of water vapor obtained by the above experimental procedure is shown in the 941–944 nm spectral region. Although the absorption spectrum of water vapor in the near infrared region has already been obtained by Gates (1960), and Streete et al. (1967), but their spectral resolution ($\geq$1 nm) are exceedingly worse than that obtained in the present work. As we can see in Fig. 2–4, the spectral resolution of about 0.05 nm is so great that every rotational line completely can be separated.

In this spectral region there are three significant absorption lines. The most intense line, centered at 944.089 nm, is caused by the ${}^{R}P_1$ rotational transition. The other two lines are due to ${}^{R}Q_2$ and ${}^{R}Q_1+{}^{R}Q_3$ rotational transitions, where the identification and notation is after Baumann and Mecke (1933).

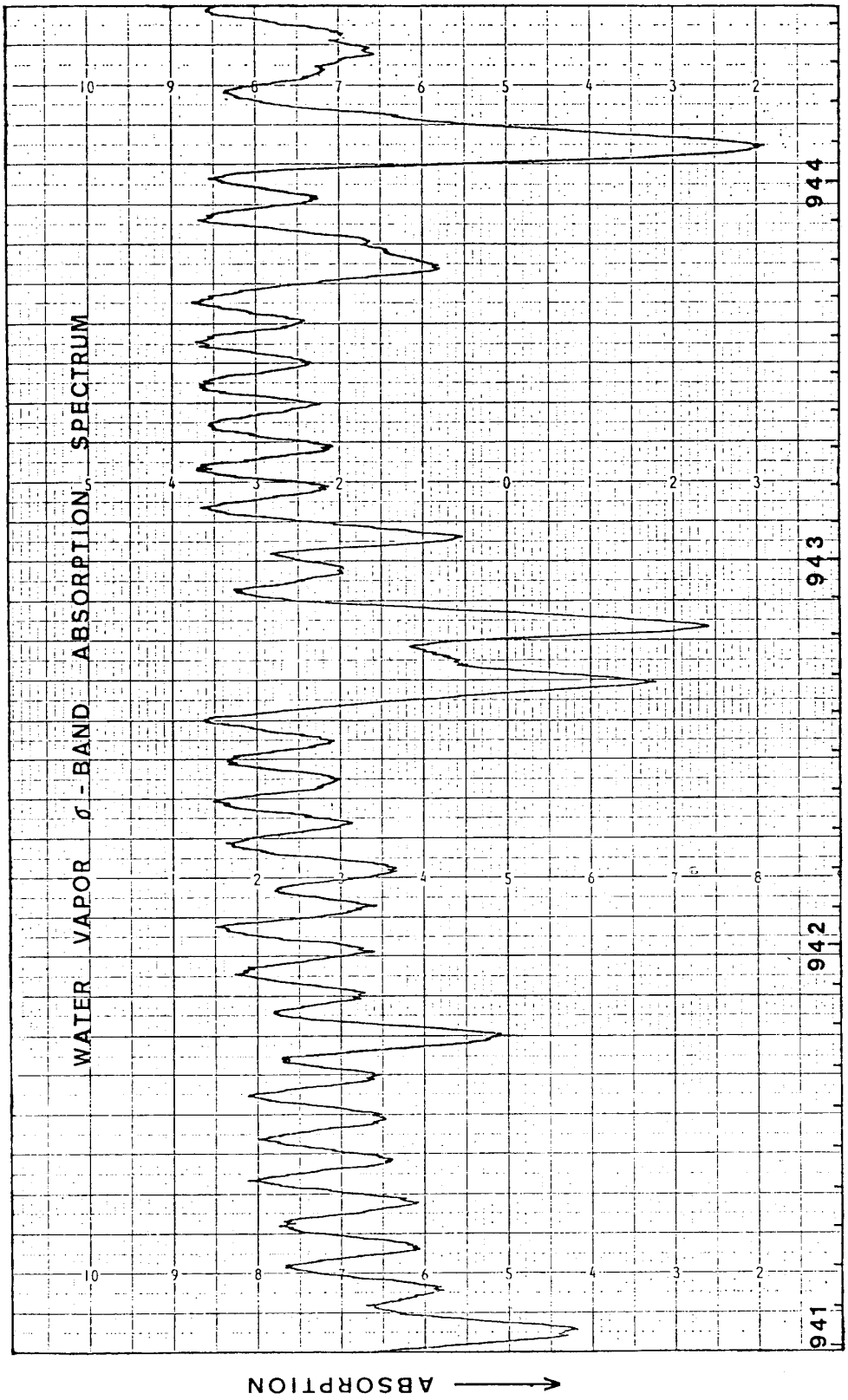

FIG. 2-4. High resolution absorption spectrum of water of water vapor in the 941-944 nm spectral region.

As will be discussed in Subsection 2.2 of Chapter III, the choice of ${}^{R}Q_2$ (2_2-2_1) and ${}^{P}Q_1$ $(1_0-1_1)+{}^{R}Q_3$ (3_1-3_0) rotational lines as absorption lines is justified for the relevant problem. Comparing the frequency of each line in Fig. 2–3 with the corresponding value given by Baumann and Mecke (1933), the intense lines agree well. However, a number of weak lines are not identified. Their origin, not to be discussed furthermore, is not clear.

2.3 *Comparison of Laboratory Spectrum with Sky Spectrum*

In order to verify that no other atmospheric absorption exists in this spectral region, the sky spectrum has to be checked. The block diagram used is shown in Fig. 2–5. Fig. 2–6 shows the sky spectrum from the 880 nm to 1000 nm spectral region.

With respect to the correspondence of each absorption line, we show the laboratory spectrum together with the sky spectrum in the spectral region of interest in Fig. 2–7. Of course, two spectra are taken with the same spectral resolution of approximately 0.05 nm. As indicated by each sign, there is almost one-to-one correspondence. Accordingly, it becomes evident that the atmospheric absorption in this spectral region is almost due to the H_2O molecules.

The open triangles indicate three strong absorption lines which have been described earlier. The center wavelengths are 942.685 nm, 942.836 nm, and 944.089 nm, respectively. The flat parts of the sky spectrum indicate the noise level determined with the dark current of the PM, i.e., in all wavelength ranges the absorption amount caused by the atmospheric water vapor exceeds 100 percent owing to its intense absorption.

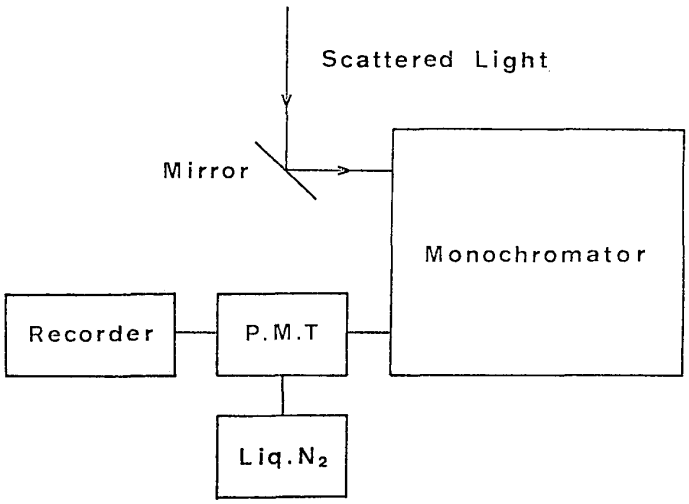

FIG. 2–5. Block diagram for obtaining a sky spectrum.

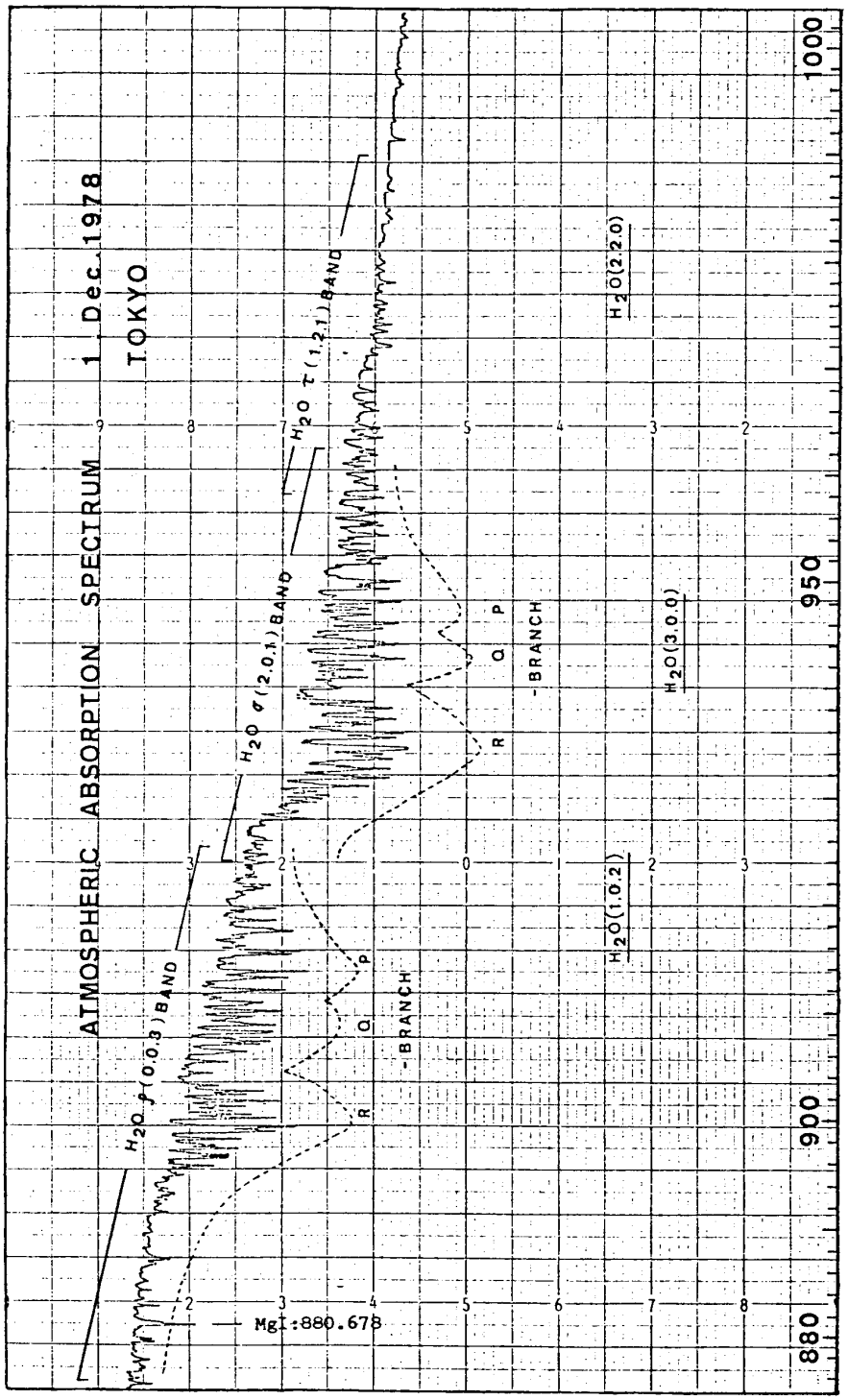

FIG. 2-6. Sky spectrum in the 880–1000 nm spectral region with H_2O ρ-, σ-, τ-band is shown in this figure.

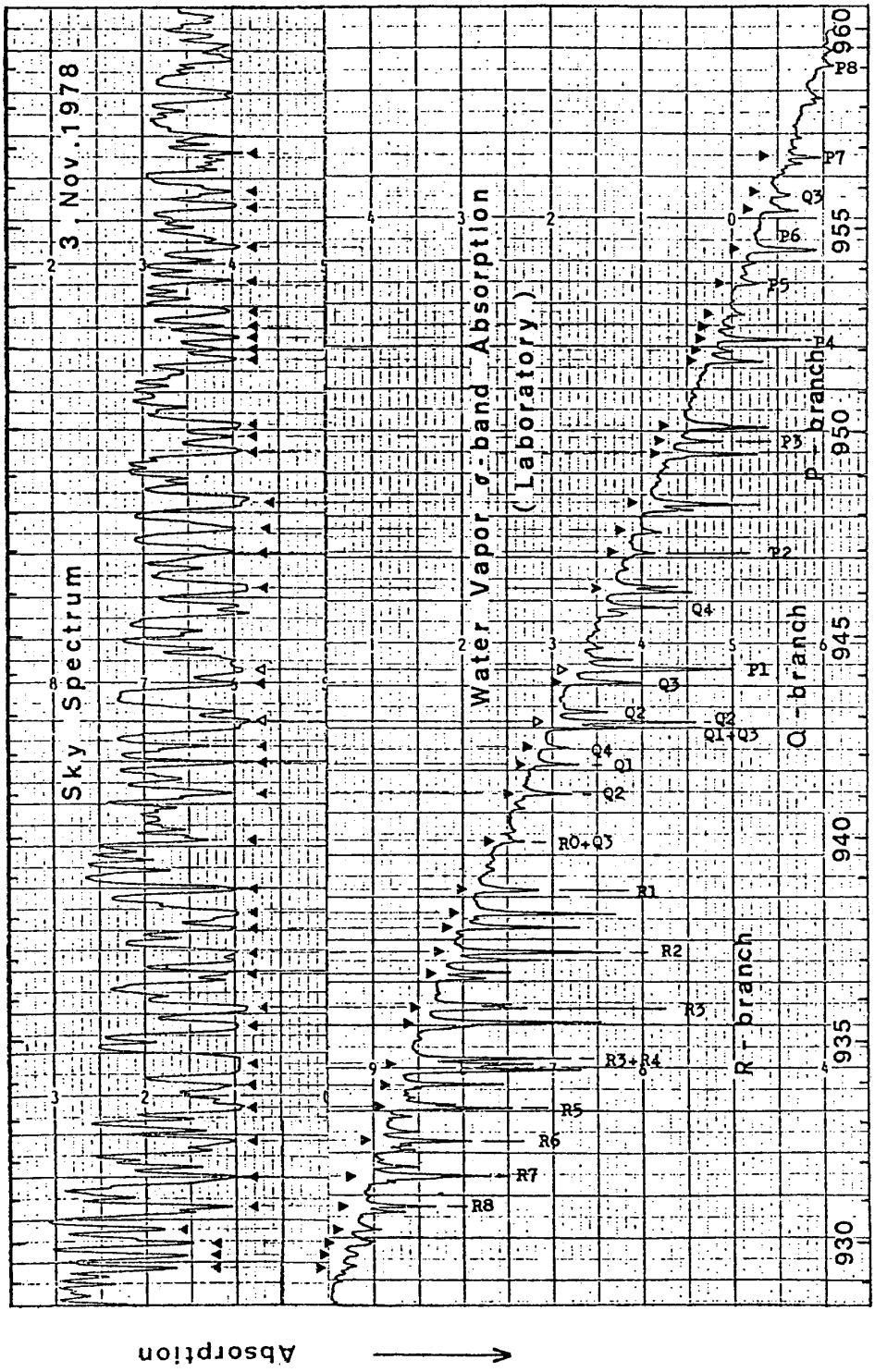

FIG. 2-7. Laboratory spectrum together with sky spectrum in the 930-960 nm spectral region.

2.4 *Discussion*

As we have seen in the preceding Sections, water vapor has a number of absorption lines in the near infrared region. From the standpoint of observing the stratospheric water vapor concentration, the strong absorption lines must be selected for tuning the center wavelength of the interference filter. The fundamental ν_1, ν_2, ν_3 modes have strong absorption bands in the wavelengths of 2.74 μm, 6.27 μm, and 2.66 μm, respectively.

However, there exists no appropriate light source in these wavelength range with high stability. In addition, numerous absorption lines of the other atmospheric molecules were superimposed on the water vapor absorption lines. For example, the NO_2 ν_3 band occurs in the center of the 6.27 μm H_2O band, though its effect is small enough to detect the water vapor density. In addition to the NO_2 band, the absorption band of molecular oxygen centered at 6.45 μm occurs due to pressure-induced effects (see for example, Williamson and Houghton, 1966). In the 2.5 μm–3 μm region intense absorption lines are existing due to two combination bands of CO_2 at 2.69 μm and 2.77 μm (Goody, 1964). Therefore we cannot use these fundamental H_2O bands inspite of their strong absorptivity.

On the other hand, with respect to the overtone and combination bands such as ϕ(1.13 μ), ψ(1.38), and Ω(1.87 μ) bands, only water vapor absorption is dominant in each spectral region. However, these wavelength bands cannot be used mainly from the problem associated with light source and the resultant radiation detector. Although a number of diode lasers with corresponding wavelengths are available, laser which we can use for *balloon experiment* is difficult to get. Further tungsten lamp which can emit these wavelength bands is available but not proper for balloon experiment mainly because of the big power dissipation of the tungsten lamp.

Accordingly, we conclude for the present problem that the choice of the σ-band absorption is most desirable at present.

§ 3. Measurements of Absorption Cross Sections in the σ-Absorption Band of Water Vapor

In this Section, we report the experimental procedure and results of measurements of water vapor absorption cross sections in the 0.94 μm region in detail. These results are useful for the evaluation of the water vapor observations in the stratosphere.

3.1 *Principle of Measurement*

We assume the light source to be completely monochromatic with wavelength λ. This monochromatic light is then attenuated by a single absorbing gas according to Lambert-Beer's law;

$$I = I_0 \exp(-n\sigma L), \qquad (1)$$

where I is the received light intensity, I_0 is the incident light intensity, n is the number density (molecules$\cdot$cm^{-3}) of the absorber in the sensing region, σ is the absorption cross section (cm$^2\cdot$molecule^{-1}) at center wavelength λ, and L is the length (cm) of the absorbing path. Although σ is actually dependent on pressure or the presence of other gases, the modification of line profile will be discussed in Subsection 3.3.

If the absorbing gas is water vapor and if I_0 is known, then the received light intensity provides a direct measure of the absorption cross section. So equation (1) yields in a simple way:

$$\sigma=\frac{1nI_0/I}{nL}. \tag{2}$$

Furthermore, if $\Delta I=I_0-I$ gives the H_2O absorption amount, σ can be determined by the following simple formula;

$$\sigma=\frac{\Delta I/I_0}{nL} \tag{3}$$

where

$$\Delta I/I_0 \ll 1.$$

3.2 *Experimental Instrumentation and Procedure*

The block diagram for this measurement is shown in Fig. 2–8. The emission spectrum of LED of a light source is indicated in the upper curve of Fig. 2–9. The lower curve of this graph shows the spectrum with a number of absorption bands or lines, i.e., ρ-band in the 900–920 nm region, σ-band in the vicinity of the center, and τ-band near 1 μm. The total power of this Ga-As LED exceeds 3 milliwatts. Therefore we may expect its radiative strength to be about 100 μw/nm, at $\lambda=940$ nm. Some features of LED are as follows:

(1) Output power is exceedingly stable,
(2) The emission peak lies in the vicinity of 0.94 μm spectral region, where the strong H_2O absorption lines exist,
(3) Rise-time of LED is so fast (~ 1 μsec) that we can easily make use of electrically chopped light,
(4) Light emitted is strongly directive.

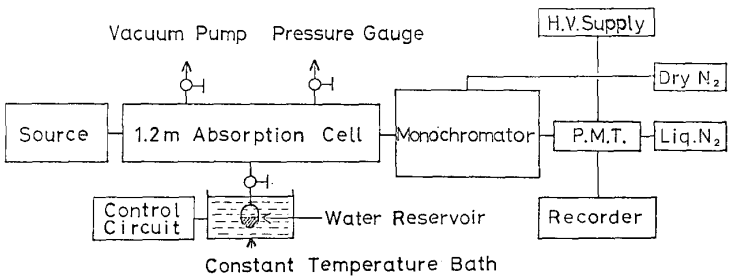

FIG. 2–8. Block diagram for measurements of absorption cross sections of water vapor in the 0.94 μm region.

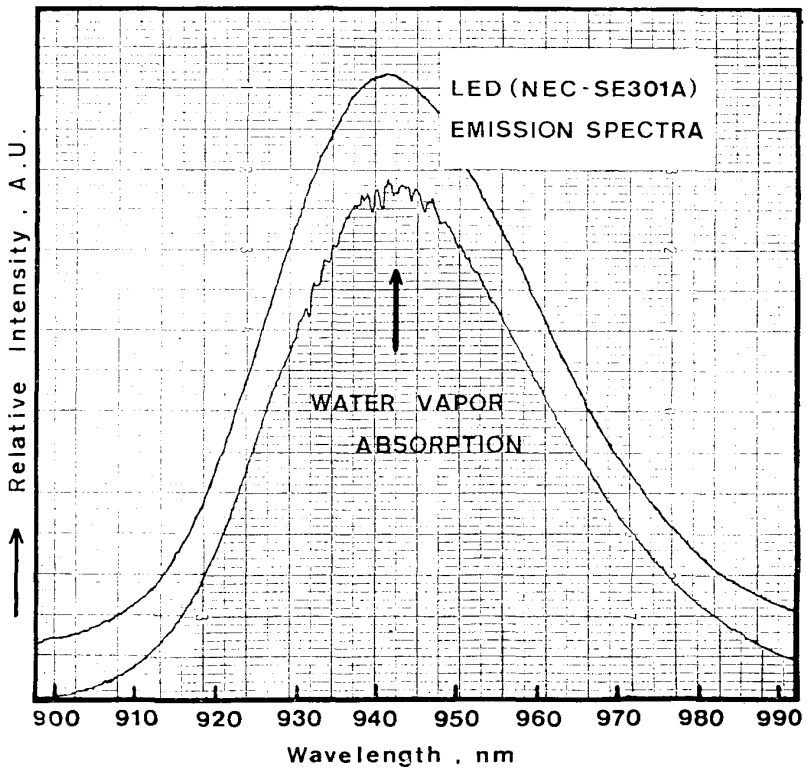

FIG. 2–9. Emission spectrum of light emitting diode (LED) with no absorption (upper curve) and with H_2O absorption (lower curve).

However, the most significant feature for the present work is its capability to determine the I/I_0 *and/or* $\Delta I/I_0$ ratio of Fig. 2–9 with good accuracy. From these aspects, LED provides the ideal source for the present purpose.

Light emitted is introduced into the absorption cell of Fig. 2–8. After the absorption cell is once pumped to vacuum to avoid the contamination, it is filled with the saturated water vapor accomplished by controlling the temperature of the constant temperature bath (Komatsu-Yamato, Coolnics, Model CTR-1B). The empty cell gives the upper spectrum of Fig. 2–9 and the cell filled with water vapor gives the lower spectrum. If the cell temperature is 20°C, that is, the saturated water vapor pressure is 17.53 mmHg, the absorption amount at the line center gives a few percent. Radiation which has passed through the absorption cell is analyzed by the spectrometer stated earlier. The other measuring conditions are almost the same as described in Section 2 of this Chapter.

3.3 *Results and Discussion*

We show the absorption cross section $\sigma(\Delta_m)$ versus spectral resolution Δ_m of the monochromator in Fig. 2–10. As we can see in this figure, absorption cross sections are measured for two strong lines, whose wavelengths are 942.836 nm and 944.089 nm. The absorption cross section is expressed by squares for the 942.836 nm line, and by triangles for the 944.089 nm line. Spectral resolution of individual line is greater

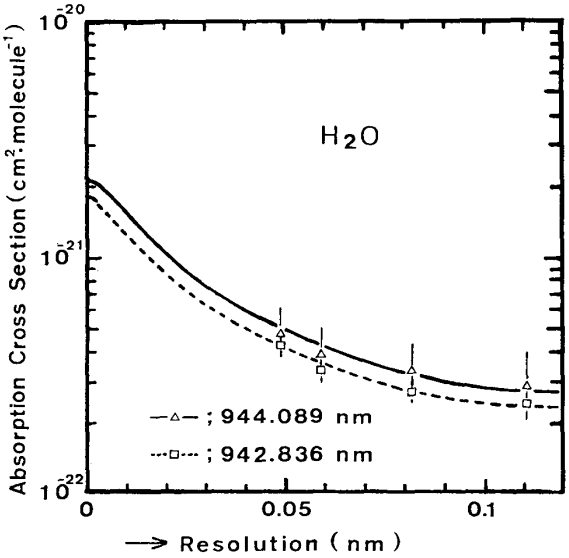

FIG. 2-10. Spectral resolution (Δ_m) of the monochromator versus absorption cross section ($\sigma(\Delta_m)$).

than 0.049 nm because of the nonlinear effect caused by a slit width narrower than about 40 μm. Therefore we have to consider the relevant absorption cross sections by means of the theoretical relations between $\sigma(\Delta_m)$ and Δ_m.

In this case, as will be seen later, the absorption spectrum of water vapor itself has the Lorentzian profile. On the other hand as the monochromator itself has the Gaussian profile, the measured spectral profile should be the Voigt profile. In the case that the spectrum has the Voigt profile, the absorption cross section at line center is given from the work of Whiting (1968) as

$$\sigma_{\lambda=\lambda_0}=\frac{\sigma_T}{\Delta_v[1.065+0.447\cdot(\Delta_s/\Delta_v)+0.058\cdot(\Delta_s/\Delta_v)^2]}, \tag{4}$$

where $\sigma_T=\int_0^\infty \sigma(\lambda)d\lambda$ is the integrated absorption cross section, Δ_v and Δ_s are the Voigt width and Lorentz width at half-height, respectively (see also Section 1 of Chapter III). Furthermore the Voigt width Δ_v is expressed as

$$\Delta_v=\frac{\Delta_s}{2}+\sqrt{\frac{\Delta_s^2}{4}+\Delta_m^2}, \tag{5}$$

where Δ_m is the Gauss width at half-height or the spectral resolution of the monochromator. Accordingly, we can get the following theoretical relation between $\sigma(\Delta_m)$ and Δ_m.

$$\sigma(\Delta_m)=\frac{\sigma_T}{\left(\frac{\Delta_s}{2}+\sqrt{\frac{\Delta_s^2}{4}+\Delta_m^2}\right)\cdot\left[1.065+0.447\cdot\frac{\Delta_s}{\Delta_s/2+\sqrt{(\Delta_s^2/4)+\Delta_m^2}}+0.058\cdot\left(\frac{\Delta_s}{\Delta_s/2+\sqrt{(\Delta_s^2/4)+\Delta_m^2}}\right)^2\right]}. \tag{6}$$

This equation should express the experimentally obtained results indicated in Fig. 2–10. In this equation, Δ_s is 9×10^{-3} nm from the work of Benedict and Kaplan (1959), so we calculated the relative absorption cross section as a function of Δ_m from eq. (6). Here the values of Δ_m are taken as 0.110 nm, 0.082 nm, 0.059 nm and 0.049 nm corresponding to those of each data point of Fig. 2–10 (Takahashi and Hirao, 1979b). From these results, we can draw the best-fit curves as shown in Fig. 2–10. The solid line represents the $\sigma(\Delta_m)$ versus Δ_m for the 944.089 nm line and the dashed line represents that for the 942.836 nm line. Since the actual spectral width is the Lorentz width of 9×10^{-3} nm, the true absorption cross sections at line center should be given by substituting $\Delta_m=0$ into eq. (6). If we assume the theoretical and experimental absorption cross section to be $\sigma_t(\Delta_m)$ and $\sigma_e(\Delta_m)$ respectively, it follows that the mean ratio of σ_t to σ_e is $3.813\sigma_T$ for the 942.836 nm line and $3.250\sigma_T$ for the 944.089 nm line. Therefore the relevant absorption cross sections can be evaluated by calculating $\sigma(\Delta_m=0)/3.813\sigma_T$ and $\sigma(\Delta_m=0)/3.250\,\sigma_T$. These calculations leads to the relevant absorption cross sections of

$$\sigma(\Delta_m)=1.86\times10^{-21}\ \mathrm{cm^2\cdot molecule^{-1}}\ \text{for the 942.836 nm line}$$

and

$$\sigma(\Delta_m)=2.18\times10^{-21}\ \mathrm{cm^2\cdot molecule^{-1}}\ \text{for the 944.089 nm line.}$$

Next, we show the other excellent methods to determine the exact absorption cross section. The Lorentzian profile of water vapor lines of interest due to collisions with other atmospheric molecules is displayed in Fig. 2–11. Because the Lorentz width of approximately 9.0×10^{-3} nm (Benedict and Kaplan, 1959) is much wider than the Doppler width of 1.6×10^{-3} nm due to the molecular thermal motions, the relevant spectral profile can be assumed to be Lorentzian. Thus, we can determine the exact value of the absorption cross sections in the following way.

In Fig. 2–12, we show the spectral transmissivity of the interference filter which was used for our stratospheric water vapor observation by balloon and four absorption lines of water vapor which should be selected for our purpose. From Lambert-Beer's law expressed in eq. (1), we obtain the following formula:

$$\frac{\Delta I}{I_0}=nL\cdot\frac{\sum_{i=0}^{N}\sigma(\lambda_i)\cdot I(\lambda_i)}{\sum_{i=0}^{N}I(\lambda_i)}, \tag{7}$$

where λ_i is the i-th wavelength as shown in Fig. 2–12, $\sigma(\lambda_i)$ is the absorption cross section at wavelength λ_i. If we denote the absorption cross section at $\lambda_s(=942.836\ \mathrm{nm})$ by σ_c and if the above-mentioned Lorentzian profile is assumed, all of the absorption cross section corresponding to each wavelength λ_i of Fig. 2–12 are directly proportional to σ_c. Therefore the convolution between the absorption cross section and light intensity at the corresponding wavelength can be expressed in the following way:

$$\frac{\sum_{i=0}^{N}\sigma(\lambda_i)\cdot I(\lambda_i)}{\sum_{i=0}^{N}I(\lambda_i)}=\frac{\sum_{j=1}^{4}\{\sum_{i=0}^{N}\varepsilon_{i,j}\sigma_c\cdot I(\lambda_i)\}}{\sum_{i=0}^{N}I(\lambda_i)}=\frac{\sum_{j=1}^{4}\{\sum_{i=0}^{N}\varepsilon_{i,j}\cdot I(\lambda_i)\}}{\sum_{i=0}^{N}I(\lambda_i)}\cdot\sigma_c$$
$$=\frac{\sum_{j=1}^{4}I_j^*}{I_0^*}\sigma_c=\frac{I^*}{I_0^*}\cdot\sigma_c. \tag{8}$$

In this expression, $\varepsilon_{i,j}$ is the above-mentioned proportional constant at λ_i belonging to the i-th absorption line. For example, $\sigma(\lambda_1)$ of Fig. 2–12 means the 1st absorption line, $\sigma(\lambda_2)$ means the 2nd absorption line, and so on. Each value of $\varepsilon_{i,j}$ is calculated from the following procedure. The relative intensity of the above four absorption lines at line center is known from the lower spectrum of Fig. 2–7. Therefore the other three absorption cross sections at line center except the 942.836 nm line can be expressed as $\varepsilon_j \cdot \sigma_c$ (ε_j: constant). Since in this case all absorption lines have the Lorentzian profile, the absorption cross section at λ_i can be reduced to $\varepsilon_{i,j} \cdot \sigma_c$ by means of the Lorentzian profile of Fig. 2–11. In addition, I_j^* and I_0^* are defined as

$$I_j^* = \sum_{i=0}^{N} \varepsilon_{i,j} \cdot I(\lambda_i), \tag{9}$$

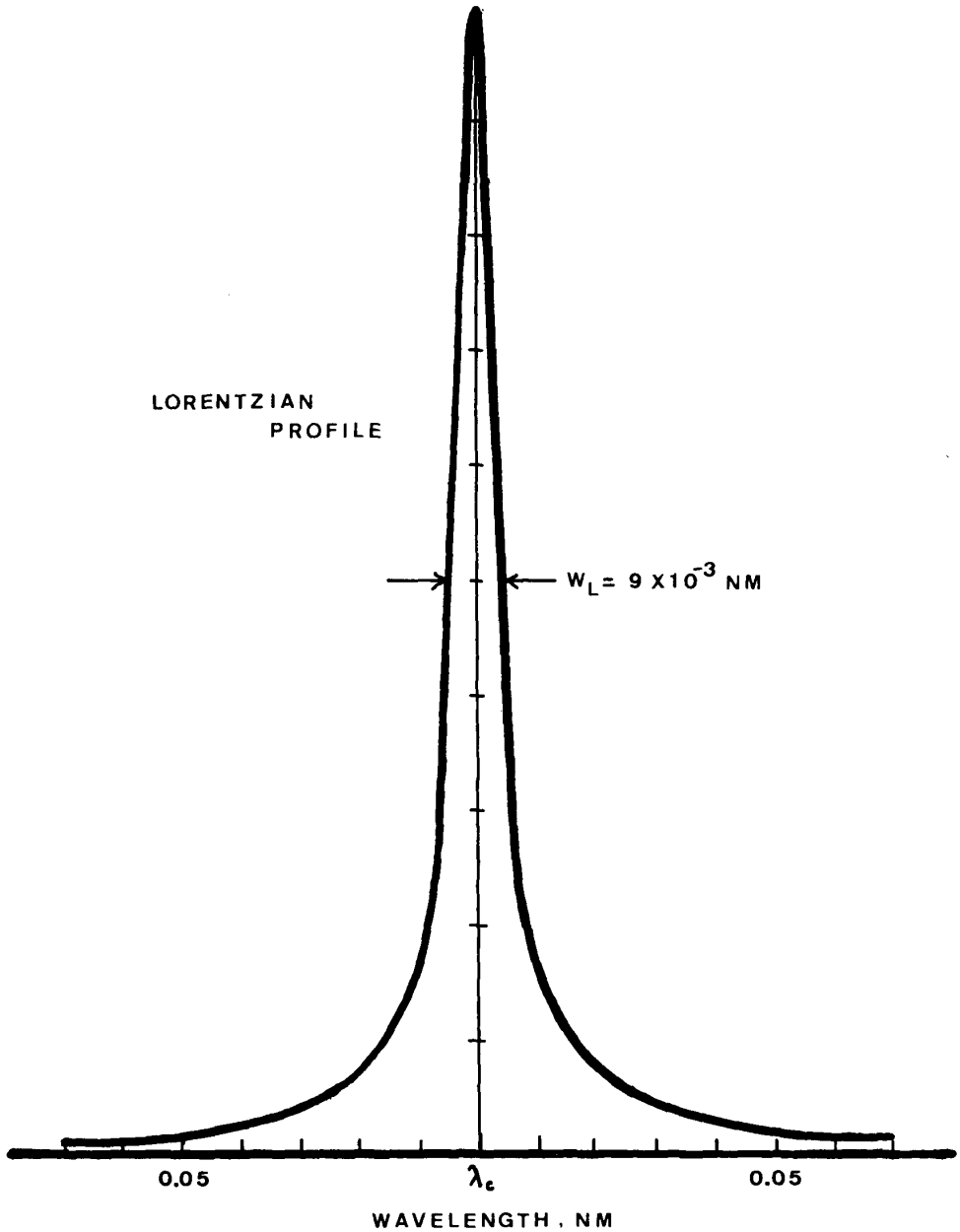

FIG. 2–11. Sketch of Lorentzian profile.

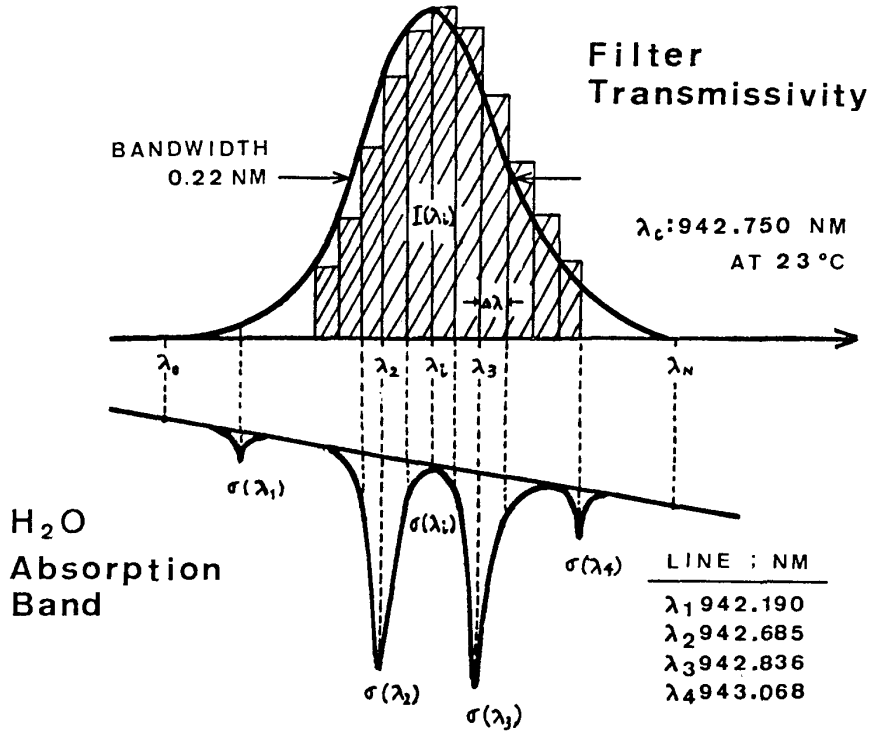

FIG. 2-12. Spectral transmissivity of interference filter and four absorption lines of water vapor.

$$I_0^* = \sum_{i=0}^{N} I(\lambda_i), \tag{10}$$

respectively. Then I^*/I_0^* is calculated by using the transmissivity curve of the interference filter shown in Fig. 3-2 and the Lorentzian profile of Fig. 2-11.

Combining eq. (7) and eq. (8), we obtain the following formula:

$$\sigma_c = \frac{I_0^*}{nLI^*} \cdot \frac{\Delta I}{I_0}. \tag{11}$$

As will be seen in Subsection 2.1 of Chapter IV, we get $\Delta I = 3.08 \times 10^4$ (counts) and $I_0 = 1.23 \times 10^6$ (counts) for the absorption amount corresponding to the water vapor which is contained in the atmosphere of an ambient temperature of 19°C and relative humidity of 60%. In addition, since $I^* = 5.70 \times 10^2$ and $I_0^* = 1.12 \times 10^4$ are calculated, we can estimate the absorption cross section at line center.

For the 942.836 nm rotational line,

$$\sigma_c = 1.64 \times 10^{-21} \text{ cm}^2 \cdot \text{molecule}^{-1}.$$

For the 944.089 nm rotational line, the absorption cross section at line center for the Lorentzian profile is estimated to be 1.78×10^{-21} cm^2 molecule^{-1}.

These values are in fairly good agreement with the values spectroscopically obtained previously.

Special attention must be paid to the fact that the absorption cross sections obtained by using an interference filter are the exact values if the Lorentzian profile as absorption profile is adopted. Even though the Voigt profile (the combination of

the Lorentz and Doppler profile) is applied, the maximum error will be less than 10 percent. Therefore a method, which uses interference filter, is exceedingly useful and effective for the determination of absorption cross section from the visible to the near infrared spectral region.

Chapter III. DETERMINATION OF WATER VAPOR CONCENTRATION IN THE ATMOSPHERE AND ITS APPLICATION TO BALLOON OBSERVATION IN THE STRATOSPHERE

§ 1. Principle for Determination of Water Vapor Concentration

The principle for determination of atmospheric water vapor concentration can be expressed again by Lambert-Beer's law:

$$I = I_0 \cdot \exp(-n\sigma L), \tag{1}$$

where the notations are the same as those described in Subsection 3.1 of the preceding Chapter. Referring to Fig. 2–12, the total intensity, I_0, tansmitted through the interference filter is given as

$$I_0 \simeq k \cdot \sum_{i=0}^{N} I(\lambda_i) \Delta\lambda \tag{2}$$

where k is the response function (constant) of the optical system, λ_0 and λ_N are the wavelengths, where the transmissivity of the filter becomes zero as shown in Fig. 2–12, and $\Delta\lambda$ is one unit of the wavelength interval of the whole transmission width of the filter divided into N wavelength intervals.

In a similar way the received intensity, I, which shows the absorption due to water vapor, can be written as

$$I = k \cdot \sum_{i=0}^{N} I(\lambda_i) \cdot \exp[-n \cdot \sigma(\lambda_i) \cdot L] \cdot \Delta\lambda. \tag{3}$$

On the other hand, the following modification

$$\begin{aligned} \Delta I = I_0 - I &= k \cdot \sum_{i=0}^{N} \{1 - \exp[-n\sigma(\lambda_i)L]\} \cdot I(\lambda_i)\} \cdot \Delta\lambda \\ &\simeq knL \cdot \Delta\lambda \cdot \sum_{i=0}^{N} \sigma(\lambda_i) \cdot I(\lambda_i) \end{aligned} \tag{4}$$

is justified for $n\sigma(\lambda_i)L \ll 1$. This condition is always fulfilled in our measurements.

Therefore, the ratio $\Delta I / I_0$ can be expressed as

$$\frac{\Delta I}{I_0} = nL \cdot \frac{\sum_{i=0}^{N} \sigma(\lambda_i) \cdot I(\lambda_i)}{\sum_{i=0}^{N} I(\lambda_i)} = nL\bar{\sigma}, \tag{5a}$$

where $\bar{\sigma}$ is considered to be the effective or mean absorption cross section when we regard $I(\lambda_i)$ as the probability function.

If we take the equation (5a) for each case of the ground-based experiment or calibration experiment and the stratospheric water vapor observation by means of the identical absorption cell, i.e.,

$$\frac{\Delta I}{I} = nL\bar{\sigma} \qquad \text{in the case of observation,} \tag{5b}$$

$$\frac{\Delta I_A}{I_A} = n_A L\bar{\sigma}_A \qquad \text{in the case of calibration,} \tag{5c}$$

then we obtain the following formula by eliminating L of eqs. (5b) and (5c),

$$n = n_A \cdot \frac{\bar{\sigma}_A}{\bar{\sigma}} \cdot \frac{\Delta I/I}{\Delta I_A/I_A}. \tag{6}$$

In this expression, n_A is the H_2O number density determined with the ambient temperature and relative humidity when the experiment is carried out. Therefore, if $\Delta I/I$ is known from the observation, we can deduce the stratospheric water vapor concentration, since in eq. (6) $n_A/(\Delta I_A/I_A)$ is given from the calibration experiment and $\bar{\sigma}_A/\bar{\sigma}$ can be calculated from the assumption of the line profile and the transmissivity of the filter as will be discussed below.

Now we have to account for the ratio of $\bar{\sigma}_A$ to $\bar{\sigma}$. Before evaluating its ratio, we will discuss on the following "Gedanken-experiment" to help our understandings. If we assume the transmission profile of the filter to be rectangular, i.e., if the light intensity in the wavelength range between λ_0 and λ_N of Fig. 2–12 is not dependent upon the wavelength, we easily see that the exact expression with respect to $\bar{\sigma}$ by using the continuous variable λ instead of λ_i of eq. (5a) is given as follows:

$$\begin{aligned}\bar{\sigma} &= \frac{\int_{\lambda_0}^{\lambda_N} \sigma(\lambda) I(\lambda) d\lambda}{\int_{\lambda_0}^{\lambda_N} I(\lambda) d\lambda} \\ &= \frac{\bar{I} \cdot \int_{\lambda_0}^{\lambda_N} \sigma(\lambda) d\lambda}{\bar{I} \cdot \int_{\lambda_0}^{\lambda_N} d\lambda} = \frac{1}{\lambda_N - \lambda_0} \cdot \int_{\lambda_0}^{\lambda_N} \sigma(\lambda) d\lambda,\end{aligned} \tag{7}$$

where $\bar{I}$ is the assumed light intensity at λ with no wavelength dependence. Consequently, equation (7) shows that for this case the absorption amount due to water vapor absorption might be dependent upon only $\int_{\lambda_0}^{\lambda_N} \sigma(\lambda) d\lambda$. Actually, this integral must be calculated for each profile of four absorption lines which have been displayed in Fig. 2–12. So we get the following expression for $\int_{\lambda_0}^{\lambda_N} \sigma(\lambda) d\lambda$;

$$\int_{\lambda_0}^{\lambda_N} \sigma(\lambda) d\lambda = \sum_{j=1}^{4} \int_{\text{line profile}} \sigma_j(\lambda) d\lambda. \tag{8}$$

Here $\int_{\text{line profile}} \sigma_j(\lambda) d\lambda$ means that the absorption cross section with the center wavelength λ_j is integrated over the wavelength range covered by its line profile. As for

these integrals, it is well known in the spectroscopy that the total absorption cross section integrated over the whole wavelength region must be constant, regardless of its line profile for an absorption line (see for example Nagata and Tohmatsu, 1973),

$$\int_{\text{line profile}} \sigma_j(\lambda)d\lambda = \frac{\pi e^2}{mc} \cdot \bar{f} = \text{constant}, \tag{9}$$

where m is electron mass, e is electron charge, c is the velocity of light, and $\bar{f}$ is the oscillator strength.

Therefore it is concluded from eqs. (7), (8), and (9) that the absorption cross section is completely independent of the atmospheric pressure and temperature, i.e., $\bar{\sigma}=\bar{\sigma}_A$ if the light intensity is constant over the wavelength range where the water vapor absorption takes place.

Next, let us consider the transmission profile of the filter as a function of the wavelength, which is the case of our present work. We know that in general the spectral profile of an absorption line depends upon the atmospheric pressure and temperature. In our case, Doppler width due to thermal motions, W_D, is calculated to be 1.6×10^{-3} nm for the temperature of 293°K (see for instance Goody, 1964), and according to Benedict and Kaplan (1959), the Lorentz width due to the collisions is about 9.0×10^{-3} nm for the standard pressure.

On the other hand, in the stratosphere the Doppler width is estimated to be 1.4×10^{-3} nm and the decrease in the atmospheric pressure and temperature leads to the Lorentz width of about 5.6×10^{-4} nm at an altitude of 20 km, since W_L is directly proportional to $(p/p_G)\sqrt{(T_G/T)}$ with respect to the pressure and temperature. In this expression, p and T are the atmospheric pressure and temperature at an altitude of 20 km ($p=55$ mb, $T=220$°K) and p_G and T_G are the same quantities at the ground ($p_G=1013$ mb, $T_G=293$°K).

From these results, it is evident that we have to treat the spectral widths with the so-called Voigt profile (Van de Hulst and Reesinck, 1947; Strong and Plass, 1950; Armstrong, 1967). Hereafter, we consider $\bar{\sigma}_A/\bar{\sigma}$ ratio by means of the Voigt spectral profile.

According to Penner (1959), the exact Voigt profile can be expressed in wavelength terms as

$$\sigma(\lambda)=\frac{2}{\pi}\cdot\frac{\lambda_0}{w_L}\cdot\sigma_p\cdot\int_{-\infty}^{\infty}\frac{\exp\left[-(2.772\,\lambda_0^2)/w_D^2\cdot(v/c)^2\right]\cdot d(v/c)}{1+(4/w_L^2)\cdot[(\lambda-\lambda_0)-\lambda_0(v/c)]^2} \tag{10}$$

where the symbols are defined as follows:

$\sigma(\lambda)$ = the absorption cross section at wavelength λ,
λ_0 = wavelength at line center,
w_L = the Lorentz width at half-height,
w_D = the Doppler width at half-height,
σ_p = a fictitious peak absorption cross section corresponding to pure thermal broadening,
c = the speed of light,

and v is integrated over all molecular velocities that may contribute to the absorption cross section at λ. To facilitate the use of this expression, several tables of $\sigma(\lambda)$ of high accuracy have been compiled (for example, Van de Hulst and Reesinck, 1947, Penner, 1959). However, even with these tables the use of the exact profile is a time-consuming process for extensive computations. Therefore, for the present purpose we adopted an empirical approximation introduced by Whiting (1968). With the following expression,

$$\frac{\sigma(\lambda)}{\sigma(\lambda_0)}=\left(1-\frac{w_L}{w_V}\right)\cdot\exp\left[-2.772\left(\frac{\lambda-\lambda_0}{w_V}\right)^2\right]+\left(\frac{w_L}{w_V}\right)\cdot\frac{1}{1+4((\lambda-\lambda_0)/w_V)^2}$$
$$+0.016\left(1-\frac{w_L}{w_V}\right)\cdot\left(\frac{w_L}{w_V}\right)\cdot\left\{\exp\left[-0.4\left(\frac{\lambda-\lambda_0}{w_V}\right)^{2.25}\right]\right.$$
$$\left.-\frac{10}{10+((\lambda-\lambda_0)/w_V)^{2.25}}\right\}, \qquad (11)$$

we can determine the absorption cross section at wavelength λ. Apparently, this equation implicitly contains the pressure and/or temperature effects in terms of the Voigt width, w_V, which is given below:

$$\text{Voigt width; } w_V=\frac{w_L}{2}+\sqrt{\frac{w_L^2}{4}+w_D^2}. \qquad (12)$$

And the absorption cross section at line center is given as

$$\sigma(\lambda_0)=\frac{\sigma_T}{w_V[1.065+0.447\cdot(w_L/w_V)+0.058\cdot(w_L/w_V)^2]} \qquad (13)$$

where $\sigma_T=\int_0^\infty\sigma(\lambda)d\lambda$ is the integrated absorption cross section. On the basis of these equations, we now can calculate $\bar{\sigma}_A/\bar{\sigma}$ in the following way,

$$\frac{\bar{\sigma}_A}{\bar{\sigma}}=\frac{\int_{\lambda_0}^{\lambda_N}\sigma_A(\lambda)\cdot I(\lambda)d\lambda}{\int_{\lambda_0}^{\lambda_N}I(\lambda)d\lambda}\Bigg/\frac{\int_{\lambda_0}^{\lambda_N}\sigma(\lambda)\cdot I(\lambda)d\lambda}{\int_{\lambda_0}^{\lambda_N}I(\lambda)d\lambda}$$
$$=\frac{\int_{\lambda_0}^{\lambda_N}\sigma_A(\lambda)\cdot I(\lambda)d\lambda}{\int_{\lambda_0}^{\lambda_N}\sigma(\lambda)\cdot I(\lambda)d\lambda}\simeq\frac{\sum_{i=0}^{N}\sigma_A(\lambda_i)\cdot I(\lambda_i)}{\sum_{i=0}^{N}\sigma(\lambda_i)\cdot I(\lambda_i)}. \qquad (14)$$

Here $\sigma(\lambda_i)$ and $\sigma_A(\lambda_i)$ both are directly proportional to σ_T from eqs. (11)–(13). Therefore if we assume those proportional constants to be k_i and $k_{A,i}$ at λ_i respectively, it follows that

$$\frac{\bar{\sigma}_A}{\bar{\sigma}}=\frac{\sum_{i=0}^{N}(k_{A,i}\sigma_T)\cdot I(\lambda_i)}{\sum_{i=0}^{N}(k_i\sigma_T)\cdot I(\lambda_i)}=\frac{\sum_{i=0}^{N}k_{A,i}\cdot I(\lambda_i)}{\sum_{i=0}^{N}k_i\cdot I(\lambda_i)}=\alpha \qquad (15)$$

In our case, this value reduced to approximately 1.06 with $w_L/w_V=0.970$ (nearly Lorentzian) for the ground and 0.327 for the 20 km-height. This fact of $\bar{\sigma}_A>\bar{\sigma}$ im-

plies that at the ground the wing effect of the Lorentzian profile is remarkable in the center of the filter transmission profile resulting in the slight decrease of the effective absorption amount for the 20 km-height. Insertion of eq. (15) into eq. (6) yields

$$n=\alpha n_A \cdot \frac{\Delta I/I}{\Delta I_A/I_A}. \tag{16}$$

In the actual observation in the stratosphere, the value $\Delta I/I$ is influenced by Rayleigh scattering by atmospheric molecules, Mie scattering by aerosol particles and the absorption by ozone. Since these effects upon the observational result are quite variable according to the height which the measurements are made, estimates on these effects will be given when the data of the observation are actually analyzed.

§ 2. Development and System Design of Measuring Instrument and Techniques

Development of the system and design of the measuring instrument and techniques are described in this Section.

2.1 *Absorption Cell and Optical System*

First we show the optical system including the absorption cell used in this experiment in Fig. 3–1. The absorption cell and the optical system were made of stainless-steel. The reason for this is as follows: (1) the vacuum for these system must be conserved under the low pressure conditions. (2) Because of the extremely

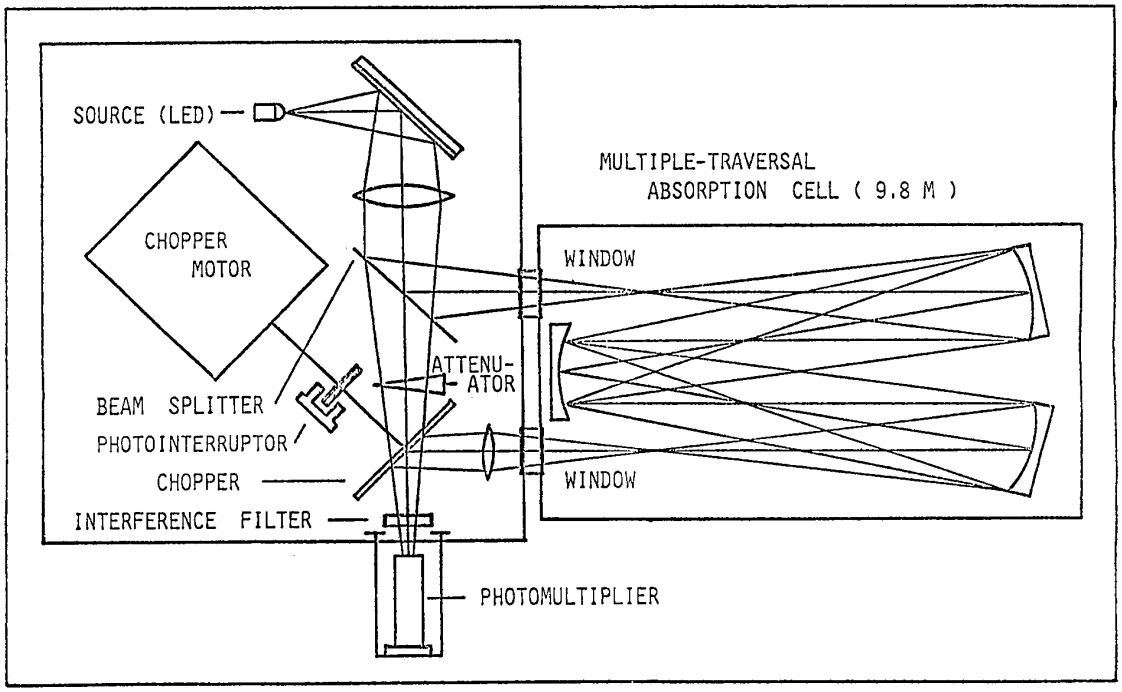

FIG. 3–1. Multiple-traversal absorption cell (path length: 9.8 m) and the optical system used in the experiment.

low temperature of the stratosphere, all optical benches must be manufactured by the materials with a small temperature coefficient. The multiple-traversal absorption cell has a 9.8 m-long absorption path by repeating 27 times reflections.

The optical system consists of the light source (LED), the chopper motor and chopper with two butterfly-type sector mirrors coated with gold, the attenuator for adjustment of the incident or reference light intensity, the interference filter, the PM tube, and some mirrors and lenses. The separation between the reference and absorbed light is accomplished by the beam slitter shown in Fig. 3–1. As for the vacuum conservation, we will describe in Section 3.

2.2 *Interference Filter*

The interference filter used for our measurements is extremely narrow band-pass filter with bandwidth of 0.22 nm. The center wavelength is 942.750 nm as we have seen in Chapter II, giving the largest absorption in the σ-band absorption. This value can be applied for the ambient temperature of 23°C.

The transmission profile is shown in Fig. 3–2. A most serious problem associated with the present filter is the ambient temperature dependence of the center wavelength. The rate of change in the center wavelength to the ambient temperature is about 0.05 nm per 1°C. Therefore to control the ambient temperature is necessary in order to reduce the shift of the center wavelength. Temperature controlling circuit which gives the accuracy of ± 0.01°C at the ambient temperature of 20°C gives the center wavelength change of $\pm 5 \times 10^{-4}$ nm. This small change of the wavelength does not affect the counting rate which will be discussed in the following Section.

2.3 *Electronic Circuitry*

This Subsection describes the detailed electronic circuitry. Fig. 3–3 shows the block diagram of electronic circuitry for measuring the stratospheric water vapor concentration.

Basic idea of the measurement system is based on the digital Lock-in method which was introduced by Terui et al. (1973) (see also Uchida and Minami, 1974; Shindoh and Baba, 1976). Though the digital Lock-in method was developed to improbe the S/N ratio of the system, a great modification was made for our purpose.

Output signal of the PM and the reference (or synchronous) signal made by a photo-interruptor (NEC, PS-4001) is shown in Fig. 3–4 (a). Duration of one measurement is 6.25 second. The chopped signals, which are shown as the upper flat level corresponding to the incident light intensity I_0 and as the lower flat level corresponding to the absorbed light intensity I are fed to the pre-amplifier every 3.125 second. Then the signals are applied to get the appropriate frequency conversion around 800 KHz by means of voltage-frequency converter (V.F.C.) without missing its linearity. These signals are digitalized and the corresponding frequencies of f_0 and f are obtained by means of the V/F converter (T.P. Model 4705). Sequentially these pulses are fed to the control gate of Fig. 3–3 which has a gate width of $T=2.063030$

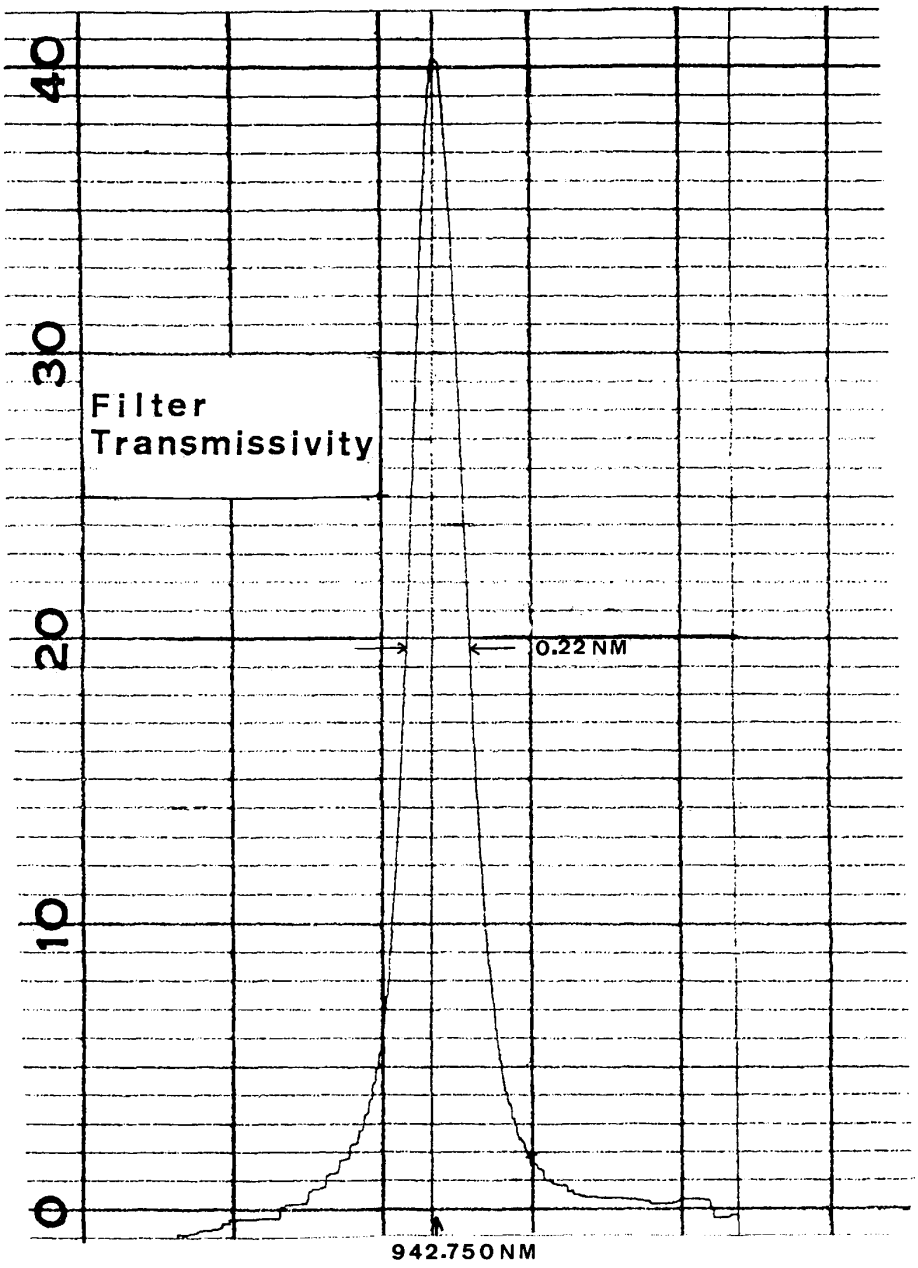

FIG. 3-2. Transmission profile of the interference filter used in this experiment.

seconds, and the above-mentioned frequencies of f_0 and f are counted during this gate width T. More detailed descriptions are given in the followings.

In Fig. 3-5(a), the number 1 of the timing chart shows the reference signal with one period of 6.25 sec from the photo-interruptor. One shot pulse indicated by the number 2 for the rise-time and 3 for the fall-time are made by the monostable multivibrators (SN 74121) shown in the left of the figure. Principally, the gate pulse indicated as 4 is obtained with the next-stage monostable multivibrator.

Since in SN 74121 the resistor and capacitor (RC) are used in order to make gate width, its highest possible accuracy becomes about 0.1 percent. Furthermore the gate

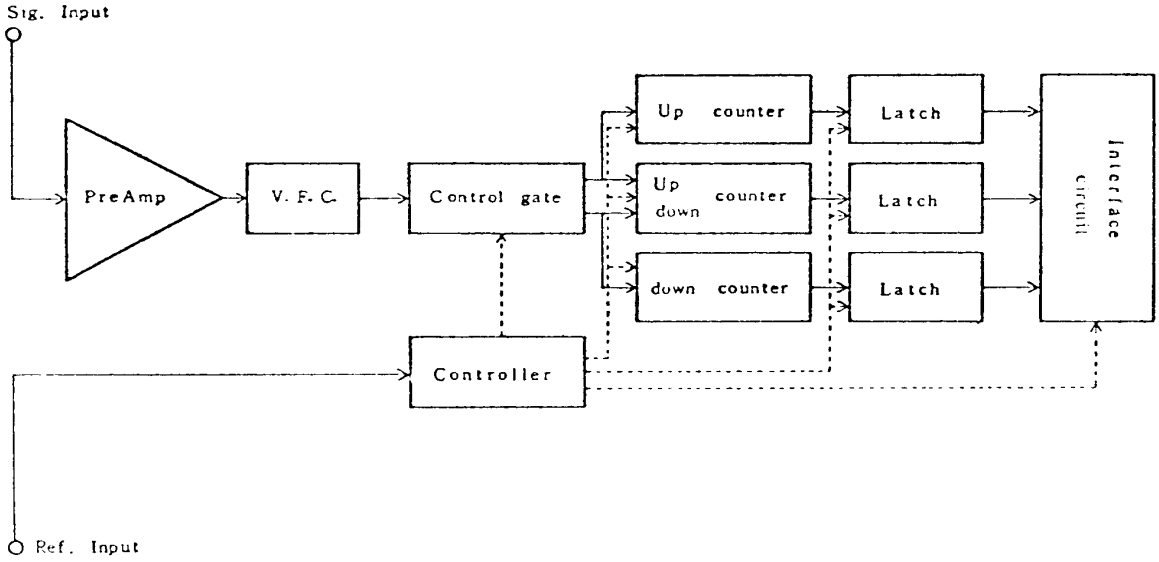

FIG. 3–3. Block diagram of electronic circuitry for measuring the stratospheric water vapor concentration.

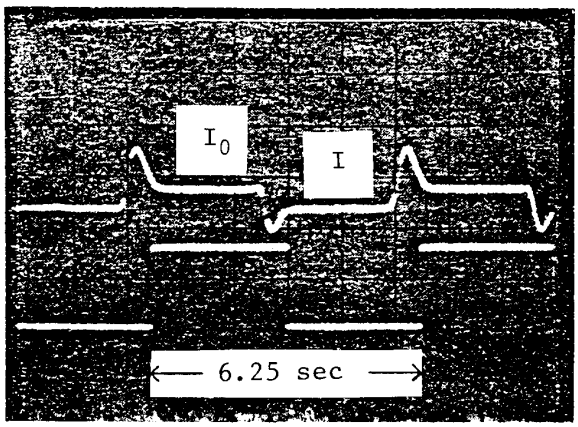

FIG. 3–4 (a). Output signal of the photomultiplier (upper part) and reference (or synchronous) signal with one period of 6.25 sec (lower part).

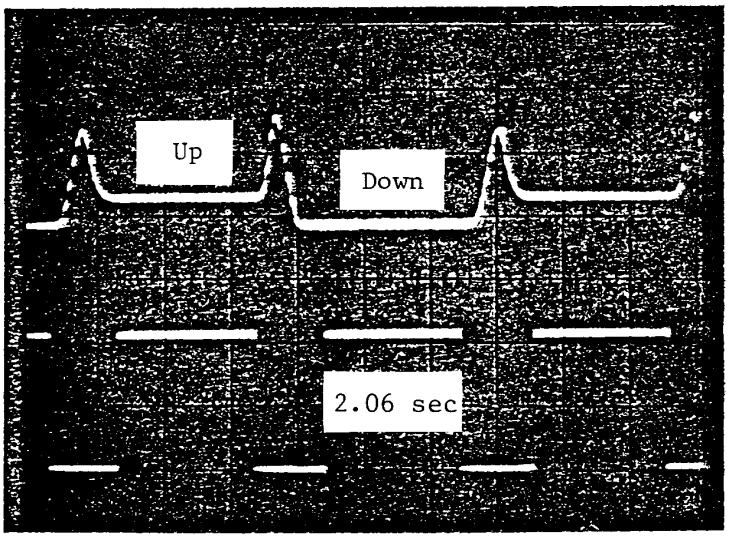

FIG. 3–4 (b). Output signal of the photomultiplier (upper part) and high accurate gate width of 2.06 sec (lower part).

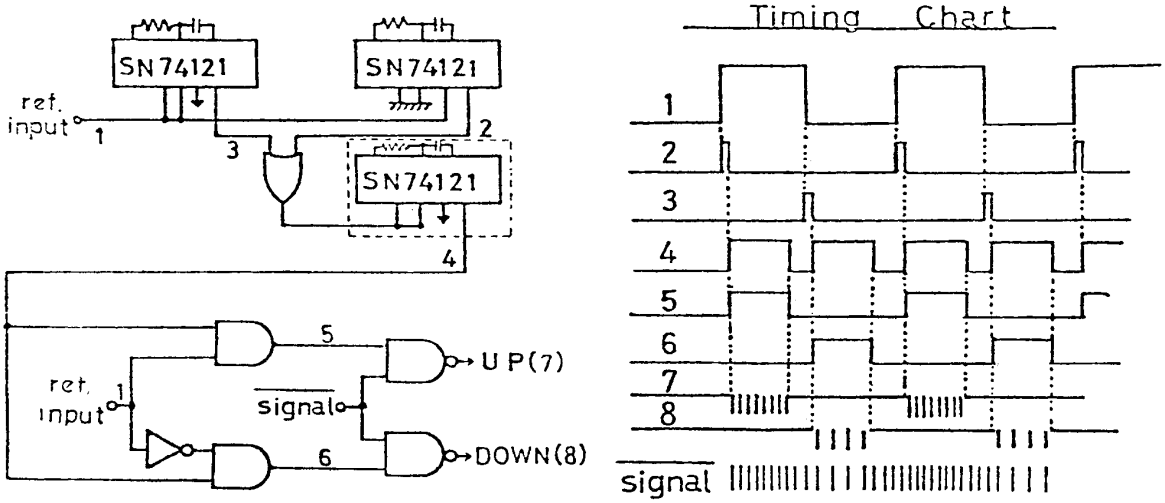

FIG. 3–5 (a). Control gate circuit (left side) and its timing chart (right side).

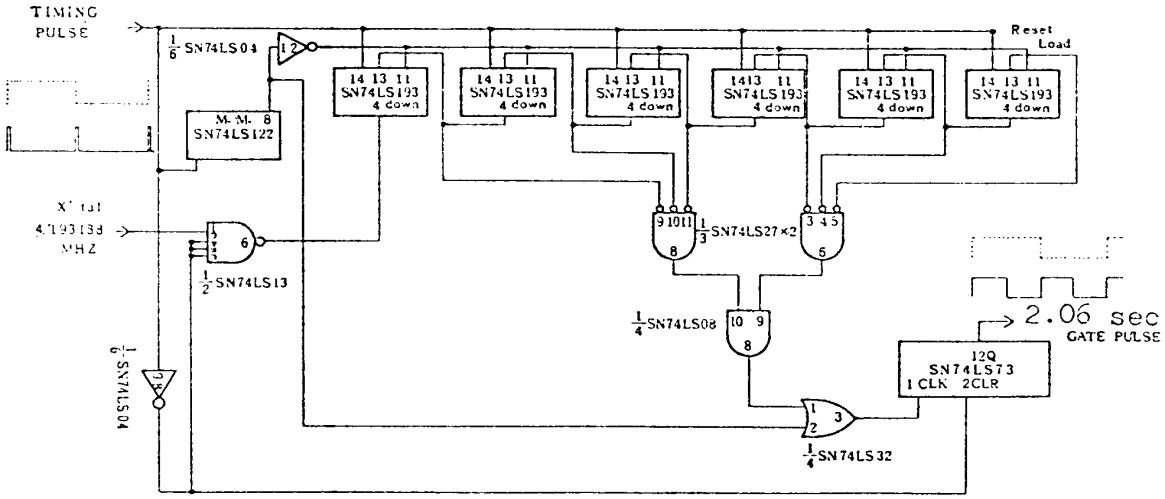

FIG. 3–5 (b). Gate pulse generator with high accuracy.

width of about 2.06 sec we need is too long to be obtained by the monostable multivibrator. In our case, this gate width will greatly affect the "true" counting rate as will be seen later, which makes us develop the high accurate circuit instead of the SN 74121 integrated circuit (IC). If we assume the stratospheric water vapor density to be several ppmV at the 20 km altitude, the accuracy of 10^{-6} is required. The accuracy of 10^{-6} is achieved by using the crystal (X'tal) oscillator and the 4-bit Up/Down counters shown in Fig. 3-5 (b). The operation of the circuit is as follows.

The outputs of the *J-K* flip-flop (SN 74LS73) are first triggered by a high-to-low-level transition of timing pulses shown by the number 2 or 3 of the timing chart. Then the output pulses (4.193188 MHz) from the X'tal oscillator are fed to the down counter of the 4-bit Up/Down counter (SN74 LS193). Here all six Up/Down counters are fully programmable; that is, each output of these counters may be preset to eigher (low or high) level by inserting the desired data. Therefore, in our case, all outputs of the counters were preset to the optimum levels which give the gate width of 2.063030 sec when all six counters are counting down to zero by 4.193188 MHz pulses. After detecting all borrow-outputs of these counters with low levels, the gate

of the *J-K* flip-flop is shut by the pulse which detected all borrows-outputs of zero or low level.

In this way we can obtain the gate width with an exceedingly high accuracy of 10^{-6}. We show above-described gate pulse of gate width T together with the output signal of PM in Fig. 3–4 (b). This gate pulse is also shown in the timing chart (number 4) of Fig. 3–5 (a). Combination of reference signal and the above gate pulse produces the gate pulse which is shown in 5 of Fig. 3–5 (a) by means of AND-logic. After inverting the logic of the reference signal, the same procedure produces the gate pulse shown in 6 of Fig. 3–5 (a). Finally, if the gate pulse of 5 and signal pulses are also fed as direct inputs to a NAND gate shown in the left hand side of Fig. 3–5 (a), the total counts of C_0, corresponding to the incident light intensity I_0, show the behavior as illustrated by the number 7 in the timing chart of Fig. 3–5 (a). In a similar way, the total counts of C, corresponding to the absorbed light intensity I, behaves as illustrated by the number 8 in the timing chart of Fig. 3–5 (a). As we can see easily, these counts are greatly affected by the above-mentioned gate width T. This is the reason why we have to develop a newly-designed circuit for making a high accurate gate width. For the sake of convenience, we will now call the counts of C_0 as "Up count" and the counts of C as "Down count" and the difference between "Up count" and "Down count", i.e., $C_0-C=\Delta C$ (which corresponds to $I_0-I=\Delta I$ as has been shown in eq. 3 of Chapter II), is called "Up-Down count".

After that "Up count" and "Down count" are counted by binary-coded decimal (BCD) counter (SN74LS90), and "Up-Down count" is counted by the BCD Up/Down counter (SN74LS192) as shown in Fig. 3–3. Then the data which are obtained in every 6.25 sec are once stored to the 4-bit memories or latches (SN74LS75), and they are transferred to the next-stage interface circuits as shown in Fig. 3–3. As for the interface circuits the detailed description will be made in Subsection 2.5 of this Chapter.

As we have seen above, in conclusion, the most significant point of our measuring circuits lies in the gate width of "Up count" and "Down count". As far as our measuring system is concerned, the accuracy of 10^{-6} for counting pulse is obtained by the circuit of Fig. 3–5 (b).

2.4 *House Keeping*

The house keeping of the scientific gondola is briefly described below. Temperature measurement of 4 points of gondora are made: (1) outside of the optical system, (2) a 5-volts regulator part, (3) the universal board of the measuring circuit and (4) the filter. The other items to be measured are: (1) the pressure of the absorption cell, (2) high voltage for photomultiplier, (3) fan motor rotation and (4) answer-backs from 4 cutter commands. In addition to the above eight items, five calibration voltage (0–5 volts) are monitored.

2.5 *Telemetry*

In this Subsection, the interface circuits as well as the telemetry system are pres-

ented. First we show the block diagram of the interface circuits in Fig. 3–6. As we have seen in Subsection 2.3 of this Chapter, "Up count", "Down count" and "Up-Down count" data are once stored in memories (or latches) of SN74LS75 indicated in Fig. 3–6. The digits of each data are 7, 7, and 5 respectively. The data are transmitted through two telemetry channels. Carrier frequency of transmitter is 1680 MHz. Subcarrier frequencies of two telemetry channels are 7.35 KHz (Channel 1) and 10.5 KHz (Channel 2) respectively. One channel (10.5 KHz) is used for the "Up count" and "Down count" data and another channel (7.35 KHz) is used for the "Up-Down count" data. Since "Up count" is stored in the memories of SN74LS75 when the level of the gate pulse becomes low (or 0), the data of "Up count" must be transmitted while "Down count" is being counted. Likewise, since "Down count" and "Up-Down count" are stored in the memories when the level of the gate pulse becomes low, the data of "Down count" and "Up-Down count" must be transmitted while "Up count" is being counted. Therefore one datum which is expressed by the binary coded decimal (BCD) count might be transmitted in sequence at 4 Hz, considering that the time-intervals of both "Up count" and "Down count" are 3.125 sec as has seen in Subsection 2.3. As for Up-Down count, one datum might be transmitted in sequence at 2 Hz. In both cases, the 8-bit multiplexers (SN74LS151) are used for this purpose. In the case of "Up count" and "Down count" data, the seven bits of the multiplexer are used for the seven digits data and the remaining bit is used as a synchronous bit. In the case of "Up-Down count" data, the five bits of the multiplexer are used for the five digits data and one bit is used as a synchronous bit and the remaining bits are always set to zero (or low level). As described above, "Up count" and "Down count" data are transmitted by switching alternatively every 3.125 sec, so that these data must be passed through the data selector (SN74LS157). Then these digital data are converted into the analog data by means of the D/A converter (Am DAC-08 EQ) in order to transmit the data by means of *FM* band. The output voltage of the D/A converter which changes from 0 V to 5 V is shifted to $-2.5\,\mathrm{V} \sim 2.5\,\mathrm{V}$ to meet the requirement of our telemetry system. In this way, we obtain the actual counts of C_0, C and ΔC on the recording paper.

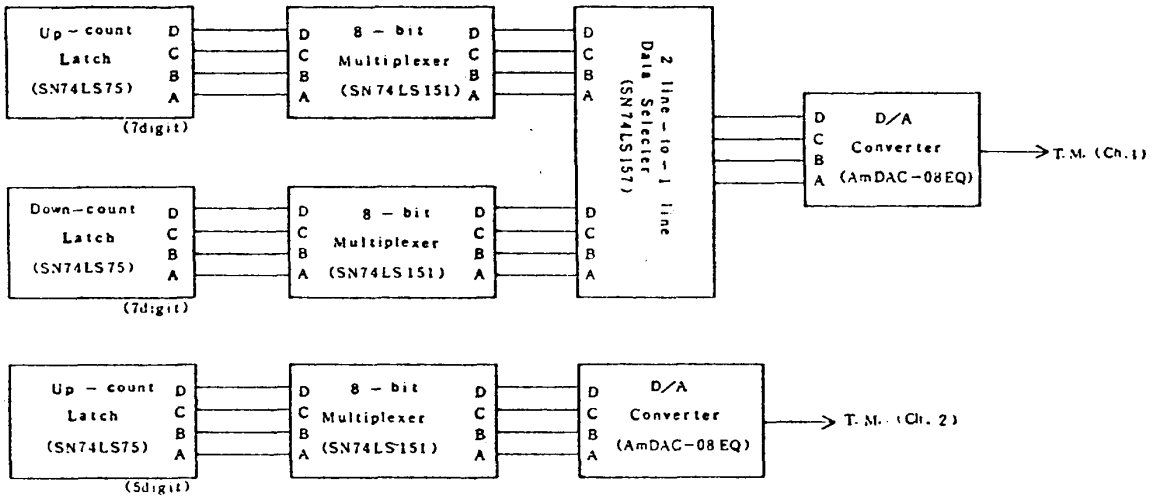

FIG. 3–6. Block diagram of interface circuits.

§ 3. Vacuum System

The outgassing from the absorption cell is of the order of $10^{12} \sim 10^{13}$ molecules$\cdot$ $cm^{-3}\cdot sec^{-1}$ when no special procedure is done for the cell system. Therefore contaminating water vapor increases up to 2×10^{13} molecules$\cdot cm^{-3}$ during one measurement (2.06 sec). On the other hand, water vapor concentration in the lower stratosphere is of the order of 10^{13} molecules$\cdot cm^{-3}$. This amount is comparable or less than contaminating water vapor of 2×10^{13} molecules$\cdot cm^{-3}$ which evaporates from the cell system. From the reason described above, the present measurement might be difficult, if no cleaning of the cell is carried out.

When the absorption cell is evacuated for three days or so, the rate of water vapor increase from the absorption cell wall becomes less than 10^{12} molecules$\cdot cm^{-3}\cdot$ sec^{-1}. During the "Down count" duration of about 2.06 sec, the contaminating water vapor increases to approximately 2×10^{12} molecules$\cdot cm^{-3}$. However, this change is negligible compared with the stratospheric water vapor density of the order of 10^{13} molecules$\cdot cm^{-3}$. Therefore we can conclude that it is required to evacuate the absorption cell system for at least three days.

§ 4. Laboratory Experiments

In this Section, we report the results of laboratory experiments carried out to confirm the operation of our measuring system.

Fig. 3–7 shows the H_2O absorption measured by the present measuring apparatus. First, we have to describe the measuring conditions by which the present measurement was carried out. The absorption cell was completely exposured in the ambient air. Then the absorption cell was pumped out to vacuum for about 1 hour. After that we stopped pumping, and began to measure.

As shown in this figure, the H_2O outgassing from the wall of the absorption cell still continues at a rate of approximately 5×10^{12} molecules$\cdot cm^{-3}\cdot sec^{-1}$. Since we obtain one "Down count" datum by counting for about 2.06 sec, outgassing rate described above produces 10^{13} molecules cm^{-3}. As this amount is comparable to the stratospheric water vapor at the height of 20 km, measurement of the water vapor gives erroneous result. Therefore it is required to evacuate absorption cell system for at least 3 days or so before balloon flight in order to reduce the outgassing during balloon flight measurement.

After ten minutes, the ambient air with the temperature of 19°C and relative humidity of 80% was introduced into the absorption cell. Then the absorption cell was pumped to vacuum again. This figure shows again that if the absorption cell is once contaminated by the ambient air, it takes a long time to clean it.

Finally as we can see in this figure, the water vapor amount in the air with the above-mentioned conditions causes the absorption corresponding to ΔI_A ("Up-Down count") equivalent to approximately 4.11×10^4 counts when the counts of the incident light intensity or "Up count", I_A, are equal to about 1.22×10^6. Therefore we can now investigate the stratospheric water vapor concentration on the basis of the present

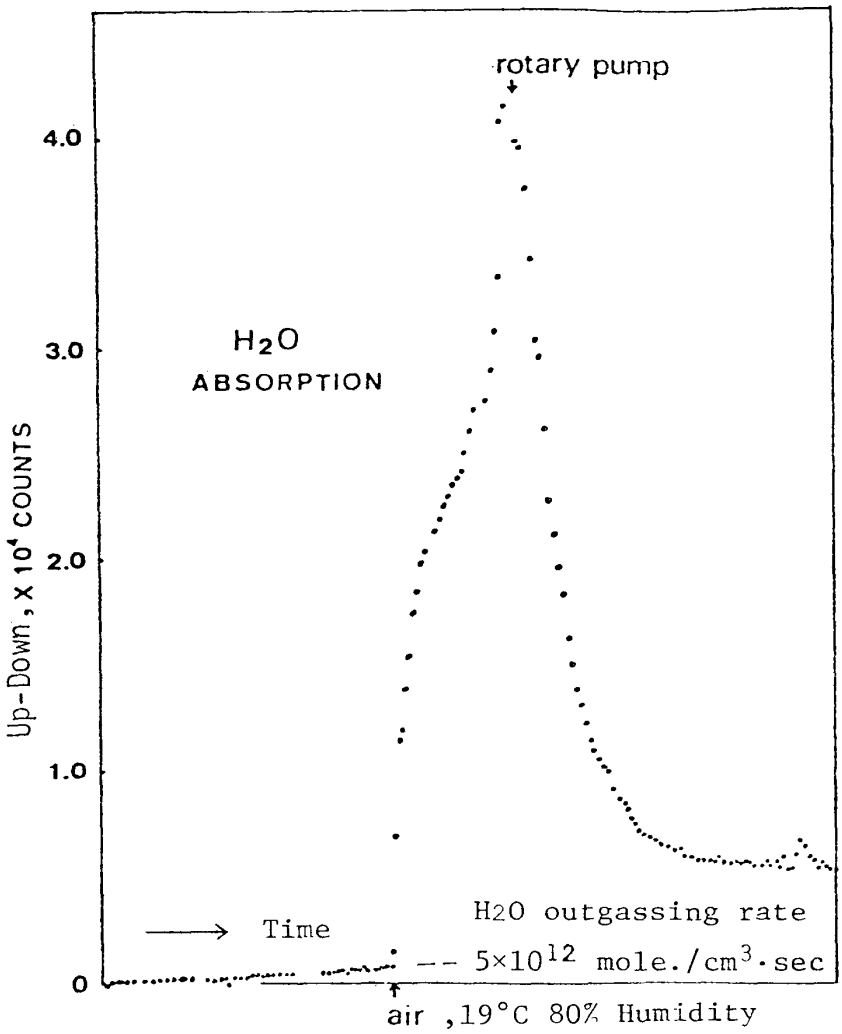

FIG. 3-7. Up-Down counts (or absorption amount) versus time. In this case, data are shown in every 12.5 sec.

calibration data. Namely, in eq. (16) of this Chapter, α, n_A, and $\Delta I_A/I_A$ are known, so that the stratospheric water vapor amount (n) can be obtained by measuring the $\Delta I/I$ ratio.

§ 5. DISCUSSION

We have seen so far the outlines of our measurement system. Optical absorption method which we have developed has several advantages over other water vapor measurement devices from the following reasons;

(a) In-situ observation of water vapor by a very simple principle,
(b) Accuracy of data which is obtained by our method is higher than any other remote sounding methods because (1) no assumption is necessary to get final data and (2) instrumental calibration which is essential to other remote sounding methods is not necessary,
(c) Water vapor observation can be done in nighttime as well as in daytime by

our method, which makes it possible to measure the variation of water vapor density in time and space.

Although more intense water vapor absorption lines exist in 1.13 μm (ϕ-band), 1.38 μm (ψ-band), and 1.87 μm (Ω-band) wavelength region, the 0.94 μm spectral region (σ-band) was used in our experiment simply because no proper light source is available for ϕ, ψ, and Ω bands at present stage. Industrial technique, however, will supply compact balloon-borne diode laser in the near future. This means that more reliable measurement is possible within several years from now by the same measurement principle which we have proposed here.

Finally, the technique which we have developed here has a extremely high counting accuracy of 10^{-6}. Therefore it can be applied to other minor constituent measurements of the upper atmosphere.

Chapter IV. BALLOON OBSERVATION IN THE STRATOSPHERE

§ 1. Introduction

This Chapter mainly describes the stratospheric water vapor observation which was done by balloon. Section 2, however, is devoted to describe ground-based experiments which are carried out before the actual balloon flight.

Section 3 describes the actual balloon flight which was carried out at the Sanriku Balloon Center, Japan.

In Section 4, the discussions are given on the data which were obtained by the balloon experiment.

§ 2. Experimental Procedure before Balloon Launching

In this Section, we discuss two ground-based experiments which should be done before actual balloon flight. One of them is the calibration of the measurement system. Information which is obtained by this experiment is used to get absolute value of the stratospheric water vapor concentration. The second procedure is the cleaning of the measurement system which consists of the absorption cell, optical system and gas inlet piping which introduce the ambient atmosphere into the absorption measurement part.

2.1 *Calibration*

This experiment was done 4 days before the actual balloon flight, since it is required to evacuate the absorption cell system for at least three days as noted earlier.

The absorption cell was evacuated for about 5 days using the cryo-sorption pump. During the evacuation, the absorption cell was heated up to $80 \sim 90°$C several times.

As a result, a pressure of 1.6×10^{-3} mmHg was achieved when the measurement started.

After we measured the absorption intensity under this condition for 10 minutes or so, the ambient air with the temperature of 19°C and relative humidity of 60% was introduced into the absorption cell. Result is shown in Fig. 4–1. As we can see

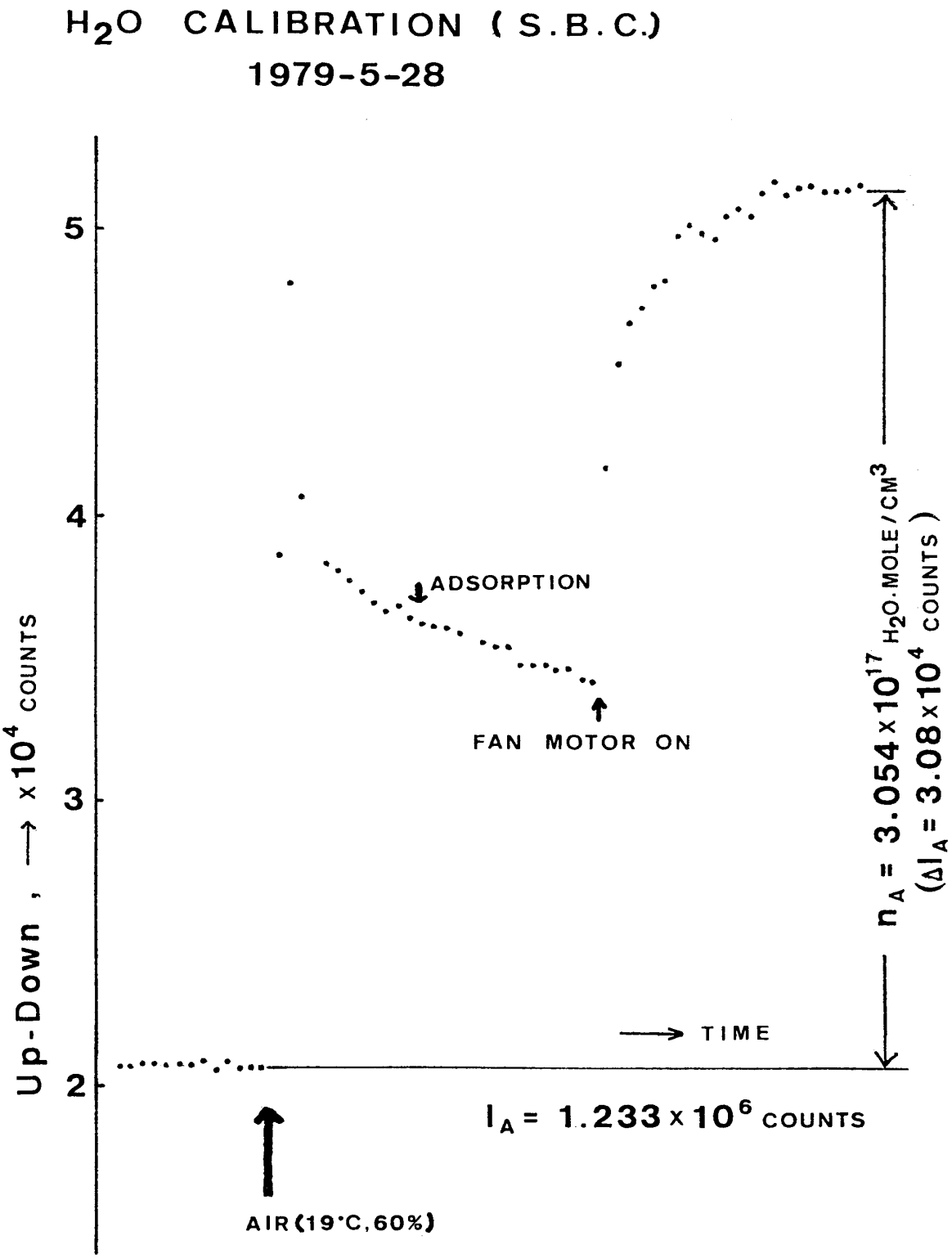

FIG. 4–1. Up-Down counts (or absorption amount) versus time. In this case, data are shown in every 12.5 sec.

in this figure, the "Up-Down" counts corresponding to the absorption due to the atmospheric water vapor are decreasing gradually because the adsorption of water vapor takes place on the surfaces of the absorption cell. 3 minutes after the fan, which circulate the air, is rotated, the "Up-Down" counts become constant because no effective adsorption takes place any longer.

From these results, it is concluded that if we take the incident light intensity, I_A, equals to 1.233×10^6 counts, the absorption amount, I, corresponding to the H_2O number density, n_A, equivalent to 3.054×10^{17} molecules$\cdot$cm^{-3} is given as 3.08×10^4 counts. (Note that n_A is calculated from the relative humidity, and the water vapor amount which is contained in a evacuated absorption cell is negligibly small compared with n_A.)

2.2 *Evacuation of the Vacuum System*

As we have discussed in Section 3 and 4 of the previous Chapter, the cleaning of the absorption cell system including gas inlet piping is of great importance for the water vapor observation in the stratosphere. After the measurement for calibration is over, the absorption cell, the optical system, and gas inlet piping were evacuated for about 4 days using the cryo-sorption pump. In particular, baking of the absorption cell and gas inlet piping was done several times. Baking temperature is 80$\sim$90°C. Thus, the rate of water vapor increase due to the outgassing from the absorption cell wall was reduced below 10^{12} molecules$\cdot$cm$^{-3}\cdot$sec^{-1}. As discussed earlier, this small outgassing rate of water vapor wiil not have any serious influence upon the experimental results.

After the baking, all of these vacuum systems are filled with dry nitrogen before the launch of the balloon, and both inlet and outlet of the measurement system are sealed by glass caps. Air is circulated by fan motor after these glass caps are removed by the command when the balloon is in the upper atmosphere.

Sketch of the B_{15}–42 balloon used for this experiment is shown in Fig. 4–2. Photograph of scientific gondola just before the balloon flight is shown in Fig. 4–3.

§ 3. Balloon Observation

The balloon observation in the stratosphere was carried out during 6/1–6/2 in 1979. The B_{15}–42 balloon has been successfully launched from the Sanriku Balloon Center (hereafter referred to as S.B.C.; 39°N, 142°E), Japan, at 17 h 52 m 43 s J.S.T. on June 1. Flight track of the balloon is shown in Fig. 4–4. The balloon flew toward the Pacific Ocean as shown in the figure. The location where the data were taken is around 38.6°N and 143°E over the sea. In Fig. 4–5 is shown the balloon height versus the time after launch. The balloon has ascended with a speed of about 250 m/sec, and it achieved a level flight at the height of about 28 km after 2.5 hours. As is well known that in most cases of the stratospheric water vapor measurements the descent data are reliable (e.g., Mastenbrook, 1968; Sissenwine, 1968; Chleck, 1979), the water vapor density was derived from balloon descending data.

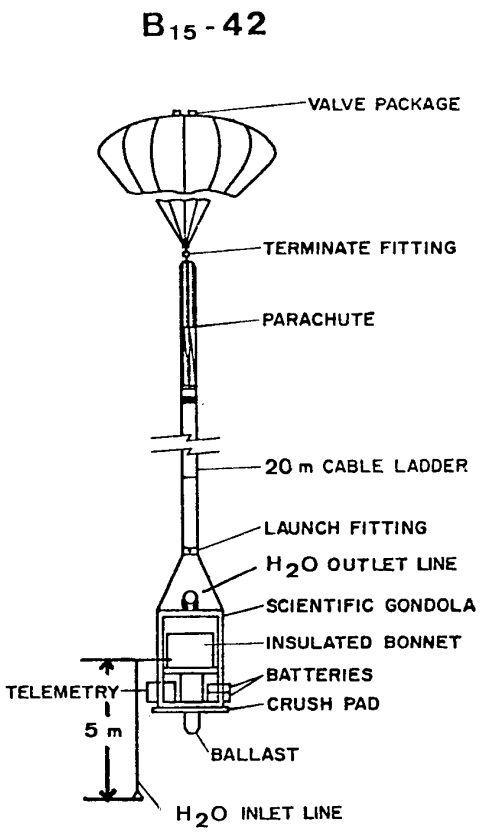

FIG. 4–2. Balloon flight train.

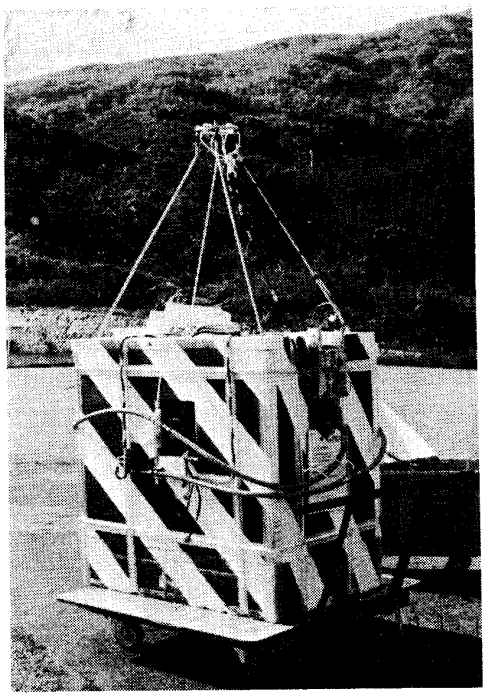

FIG. 4–3. Scientific gondola just before the balloon flight.

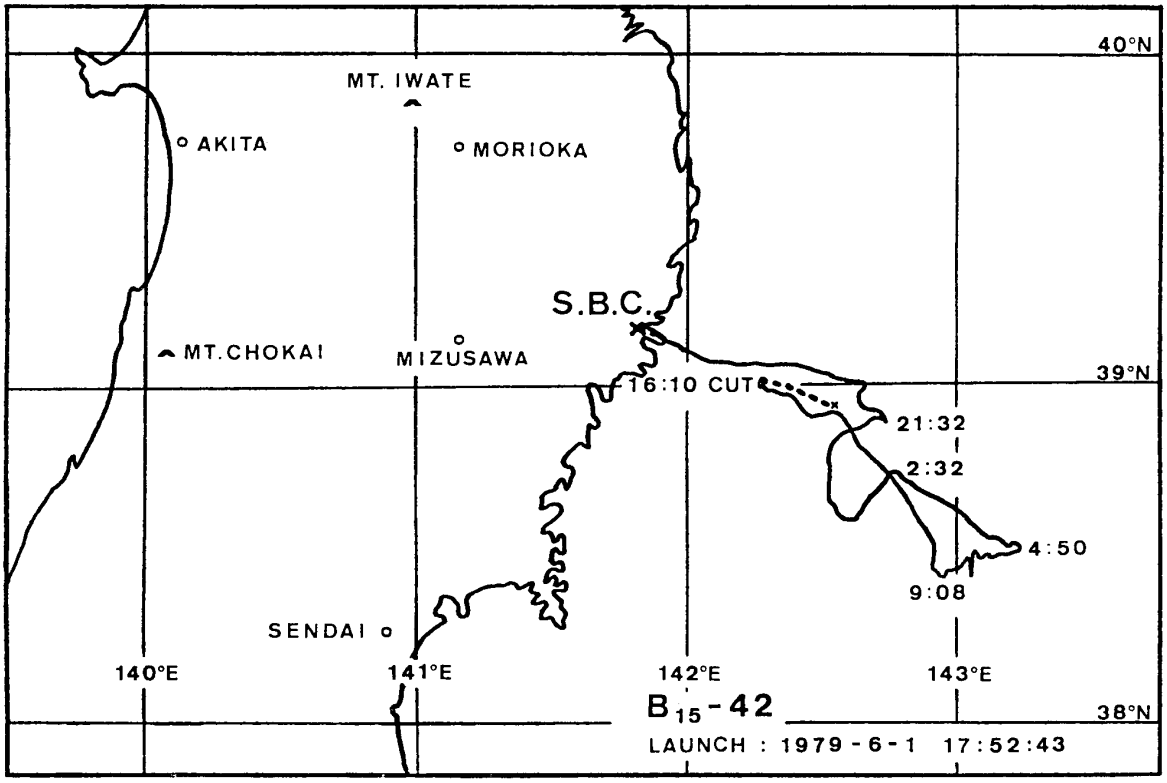

FIG. 4–4. Flight track of B_{15}–42 balloon.

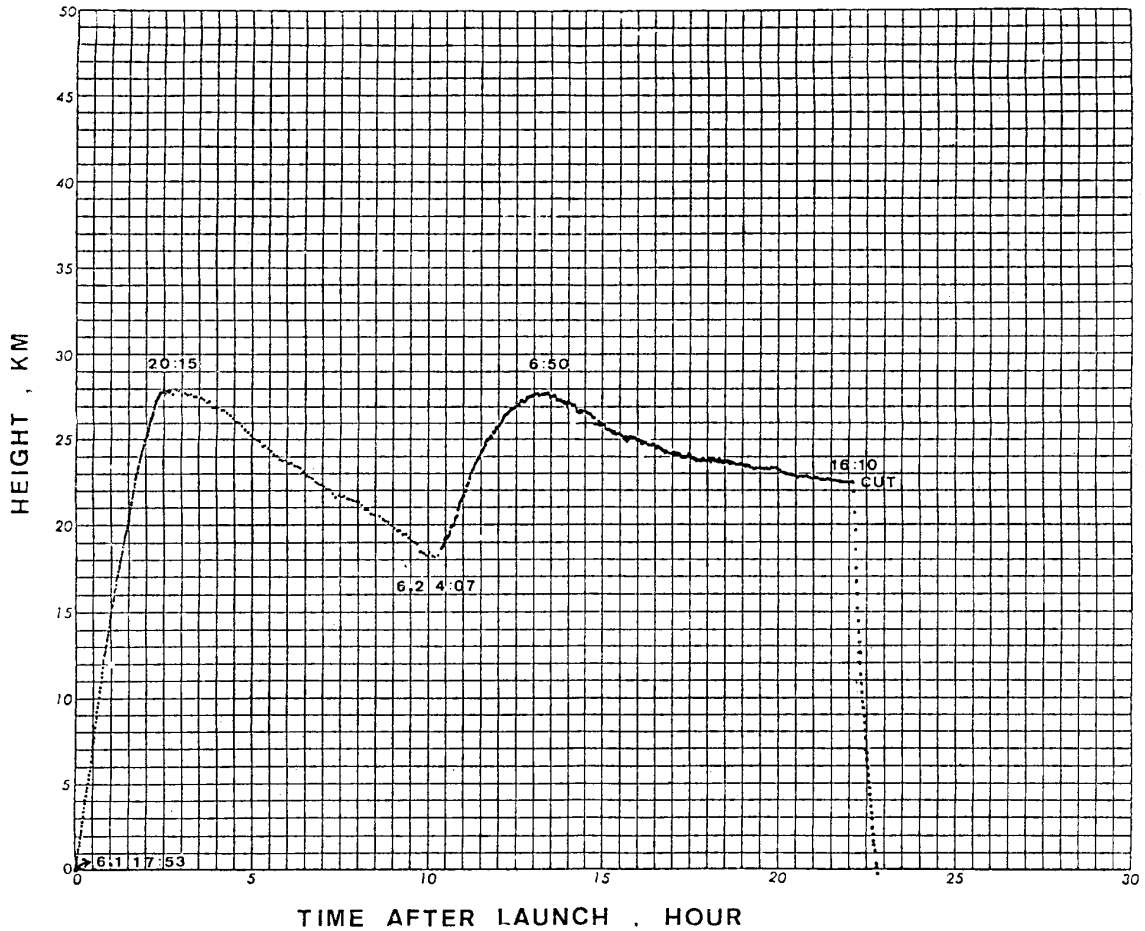

FIG. 4–5. Balloon height versus time after launch.

§ 4. Experimental Results and Discussion

In this Section, we present and discuss the results obtained by the observation together with aerological data which was obtained at the Sendai District Meteorological Observatory (hereafter referred to as S.D.M.O.) located about 125 km South-West from S.B.C. during the same period.

We also discuss the contamination from balloon and/or scientific gondola.

The water vapor content in the lower stratosphere is discussed from the standpoint of its flow process from the troposphere into the lower stratosphere in the final part of this Section.

4.1 *Data Processing*

First, we have to consider the values of $\Delta I/I$ in eq. (16) of this Chapter. To begin with, the 248, 177, and 150 "Up-Down count" data have been averaged in the altitude range of 18.2—19.0, 19.0—19.8, and 19.8—20.5 km respectively. Then we obtained the average counts of 10.48, 5.80, and 8.50 for respective heights. Since I equals to 1.56×10^{6} counts in this observation, $\Delta I/I$ reduces to 6.72×10^{-6}, 3.72×10^{-6}, and 5.45×10^{-6} for respective heights.

As already described in Section 1, the $\Delta I/I$ values are not attributed only to the water vapor absorption. For the altitude range between 18 and 21 km, it is necessary to estimate the effects of the Rayleigh scattering by atmospheric molecules, the Mie scattering by aerosols, and the weak absorption by stratospheric ozone. Next we wiil evaluate these effects below.

(a) Rayleigh scattering

According to Dalgarno (1962), the Rayleigh scattering cross section at wavelength λ_μ (micron) can be expressed as

$$\sigma_R = \frac{3.7758\times 10^{-28}}{\lambda_\mu^4}\cdot\left(1+\frac{0.00567}{\lambda_\mu^2}\right)^2 [\mathrm{cm}^2\cdot \mathrm{molecule}^{-1}].$$

Therefore we can estimate the Rayleigh scattering cross section at 0.94275 μm (at center of the interference filter) to be 4.8411×10^{-28} ($\mathrm{cm}^2\cdot\mathrm{molecule}^{-1}$). Since the path length (L) which light sustains the scattering is 9.8 m and the air densities (n_R) at respective heights are known from the radiosonde observation by S.D.M.O., we can calculate $(\Delta I/I)_R$ values which equals to $n_R\sigma_R L$ caused by the Rayleigh scattering. These values at respective heights are shown in Table 2.

(b) Mie scattering

We have the so-called Junge (aerosol) layers at about 18 km altitude (Iwasaka and Isono, 1977; Ishikawa et al., 1979) and 20 km altitude (Hirono et al., 1974) over Japan. After the eruption of Fuego volcano in Guatemala in 1974 (Fujiwara et al., 1975), the volcanic dust is the lower stratosphere has obated year after year and in 1978 the aerosol concentration is believed to be back to a stable level of the pre-volcanic aerosol layer (Hirono et al., 1979). From the work of Hirono et al. (1979), the extinction coefficients of the Mie scattering at 694.3 nm are 2.0×10^{-9}, 1.5×10^{-9},

TABLE 2.

Altitude (Km)	[Air] (mole. cm^{-3})	Rayleigh scatt. $[n_R\sigma_R L]$	Mie scatt. $[\beta_M \cdot L]$	Ozone abs. $[n_{oz}\sigma_{oz}L]$	$(\Delta I/I)_{RMO}$ [Total]
18.2 | 19.0	2.374(18)	1.13(−6)	1.44(−6)	0.07(−6)	2.64(−6)
19.0 | 19.8	2,116(18)	1.00(−6)	1.08(−6)	0.09(−6)	2.17(−6)
19.8 | 20.5	1.768(18)	0.84(−6)	1.16(−6)	0.16(−6)	2.17(−6)

cf. $a(-p)=a\times10^{-p}$

and $1.7\times10^{-9}\,cm^{-1}$ at about 18.6, 19.4, and 20.2 km height, respectively, Pinnick et al. (1976) found that the scattering cross section for a typical aerosol distribution should vary as λ^{-1} (λ: wavelength) and that this wavelength dependence is relatively intensitive to the parameters of the size distribution (see also Clemesha and Simonich, 1978). From these results, we can estimate the extinction coefficient (β_M) at about 18.6, 19.4, and 20.2 km height for the 942.75 nm light to be 1.47×10^{-9}, 1.10×10^{-9}, and $1.25\times10^{-9}\,cm^{-1}$ respectively. Accordingly, we can get $(\Delta I/I)_M$ values which equals to $\beta_M L$ caused by the Mie scattering in Table 2.

(c) Absorption by ozone

Though we have seen earlier that no absorption band of other atmospheric molecules exists in the 0.94 μm spectral region, there is a weak absorption belonging to the Chappius absorption band of ozone. Since we have no information on the absorption cross section of ozone (σ_{oz}) in the relevant wavelength region, we adopt the value of $3\times10^{-23}\,cm^2\cdot molecule^{-1}$ by Ogawa (1979). The ozone number density (n_{oz}) in the altitude range of interest is well known from the data obtained by the balloon-borne *KI* electrochemical ozone sondes. In the stratosphere below 35 km the ozone concentration is said to have the stable distribution with time (Watanabe and Tohmatsu, 1976), so that we might take the mean values of atmospheric ozone concentration at respective heights. Following Watanabe and Tohmatsu (1976), if we take the ozone number density of 2.5×10^{12}, 3.0×10^{12}, and 3.3×10^{12} at 18.6 km, 19.4 km, and 20.2 km height respectively, we can obtain the $(\Delta I/I)_{oz}$ values by calculating $n_{oz}\sigma_{oz}L$ at respective height in Table 2.

We have evaluated three effects which have influence upon the observational result above. We give the total effect which is expressed as $(\Delta I/I)_{RMO}$ in the last column of Table 2.

From these results, we can deduce the water vapor concentration from eq. (16), since the absorption due to atmospheric water vapor should be given as

$$\Delta I/I=(\Delta I/I)_{Obs.}-(\Delta I/I)_{RMO},$$

where $(\Delta I/I)_{Obs.}$ denotes the observed values which have described earlier. The water

TABLE 3.

Altitude (km)	Press. (mb) Tem.(°C)	No. of data	$\left(\frac{\Delta I}{I}\right)_{\text{Osb.}}$	$\left(\frac{\Delta I}{I}\right)_{\text{RMO}}$	$[H_2O]$ No. density (cm^{-3})	Volum Mixing Ratio (ppmV)	Saturation Mixing Ratio (ppmV)	Relative Humidity (%)
18.2	70	248	+4.03	+0.36	+5.69	+22.0	151.3	14.7
|			6.72(−6)	2.64(−6)	5.29(13)	22.3		
19.0	−56.6		−4.03	−0.36	——	——		
19.0	63	177	+2.99	+0.36	+4.34	+20.5	194.1	4.9
|			3.72(−6)	2.17(−6)	2.01(13)	9.5		
19.8	−55.5		−2.99	−0.36	——	——		
19.8	53	150	+6.05	+0.36	+8.31	+47.0	262.0	9.1
|			5.45(−6)	2.17(−6)	4.25(13)	24.0		
20.5	−54.5		——	−0.36	——	——		

cf. $a(-p)=a\times 10^{-p}$

vapor concentrations obtained in this observation are tabulated in terms of the number density (molecules·cm^{-3}) and volume mixing ratio (ppmV) in Table 3. The data of the atmospheric pressure and temperature are obtained by the radiosonde observation flown from S.D.M.O. during the same period as our balloon observation. In this table, the probable error of $(\Delta I/I)_{\text{Obs.}}$ is inferred from the standard deviation of the statistical fluctuation of the counts, because the errors resulted from the determination of α and n_A in eq. (16) are sufficiently small compared with the statistical fluctuation of the counts. On the other hand, uncertainty of $(\Delta I/I)_{\text{RMO}}$ values is mainly derived from the term of the Mie scattering, because the effects resulted from the ambiguity concerning the Rayleigh scattering and the absorption by ozone are sufficiently small. The erroneous ranges of $(\Delta I/I)_{\text{RMO}}$ which are shown in Table 3 are determined with the maximum and minimum values of the extinction coefficients which have been so far obtained by the Japanese research groups (Hirono et al., 1972, 1974, 1979; Iwasaka and Isono, 1977; Itabe et al., 1977; Ishikawa et al., 1979). Total effects on the errors of this measurement are shown in Table 3.

As shown in Table 3, the volume mixing ratios obtained in this observation are about 22, 10, and 24 ppm for the heights of 18.6, 19.4, and 20.2 km respectively. According to Stanford (1974), the saturation mixing ratio is given by

$$r_i(p, T)=\frac{0.622\, e_i(T)}{p-e_i(T)},$$

where p is the atmospheric pressure at the altitude of interest and $e_i(T)$ is the saturation vapor pressure of water vapor over ice at temperature T. The $e_i(T)$ values were obtained from the Tables in the text of Goody (1964). Based on this, we calculated the saturation mixing ratio at the altitude of interest. As we can see in the column of this Table, the saturation mixing ratio ranges between 151 and 262 ppmV. The relative humidities, therefore, at the heights of 18.6, 19.4, and 20.2 km are approximately 15, 5 and 9% respectively. These results are shown in Fig. 4–6 together with the other in-situ data obtained by Mastenbrook (1968, 1971) and Sissenwine et al.

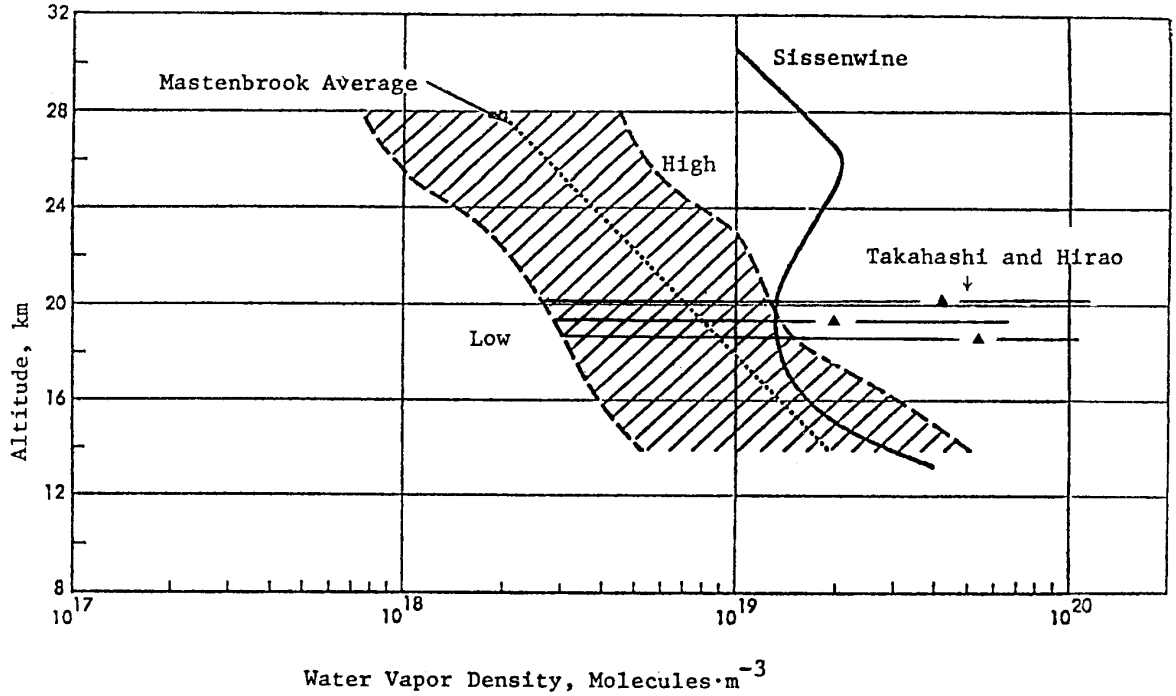

FIG. 4–6. Altitude distribution of water vapor in the stratosphere obtained by this observation.

(1968). Apparently our result shows higher water vapor concentration than those obtained by Mastenbrook and Sissenwine.

Aerological data are shown to examine the atmospheric conditions in the lower stratosphere and troposphere in the following.

In Fig. 4–7, is shown the relative humidity below the tropopause as well as some examples of the water vapor observation in the lower stratosphere. These humidity data were taken by the radiosonde flown from the S.D.M.O. during the same period. It is evident from this figure that at least below the tropopause the atmosphere has become exceedingly moist with time. The rate of increase in the relative humidity comes to about twice per 12 hours. This implies that there was a flow of the moist air mass before our observation. As will be seen later, this fact is verified also in terms of the atmospheric temperature.

In Fig. 4–8, is shown the data of the atmospheric temperature obtained by the above-mentioned radiosonde. The figure shows the remarkable change in temperature with time. The temperature profile expressed by the dotted line is most typical one except a slight increase at an altitude of 14 km. As we can easily see in this figure, the region 15–21 km of interest indicates the uniform decrease of 4–5°C with time, regardless of day or night. In the altitude range between the first tropopause around 11 km and second tropopause around 15 km, drastic change takes place. The uniform increase in temperature reaches about 8°C per 36 hours. On the contrary, the temperature below the first tropopause is uniformly decreasing with time at the rate of about 2°C/day. In addition, the temperature profiles in this region are showing almost moist-adiabatic lapse rate. This leads again to the suggestion that there was a flow of the moist air mass at this period.

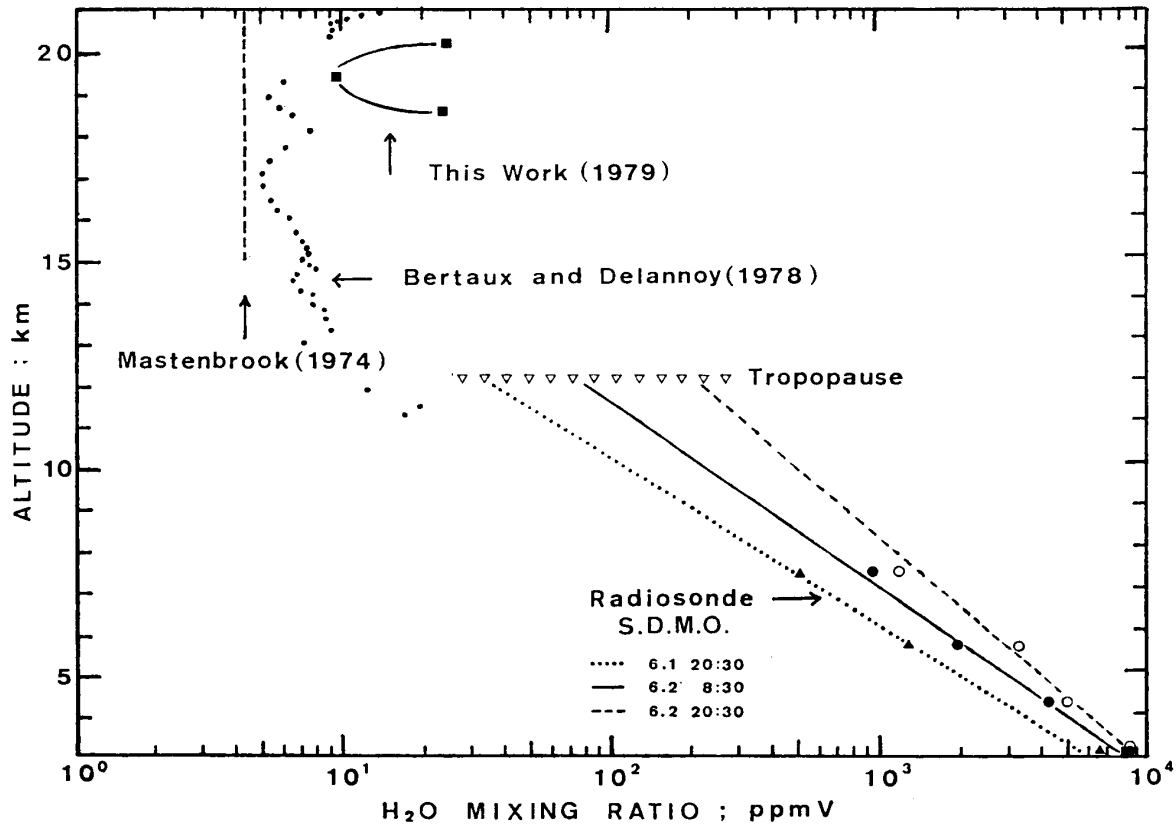

FIG. 4–7. Altitude distribution of water vapor in ppm unit together with the aerological data at Sendai.

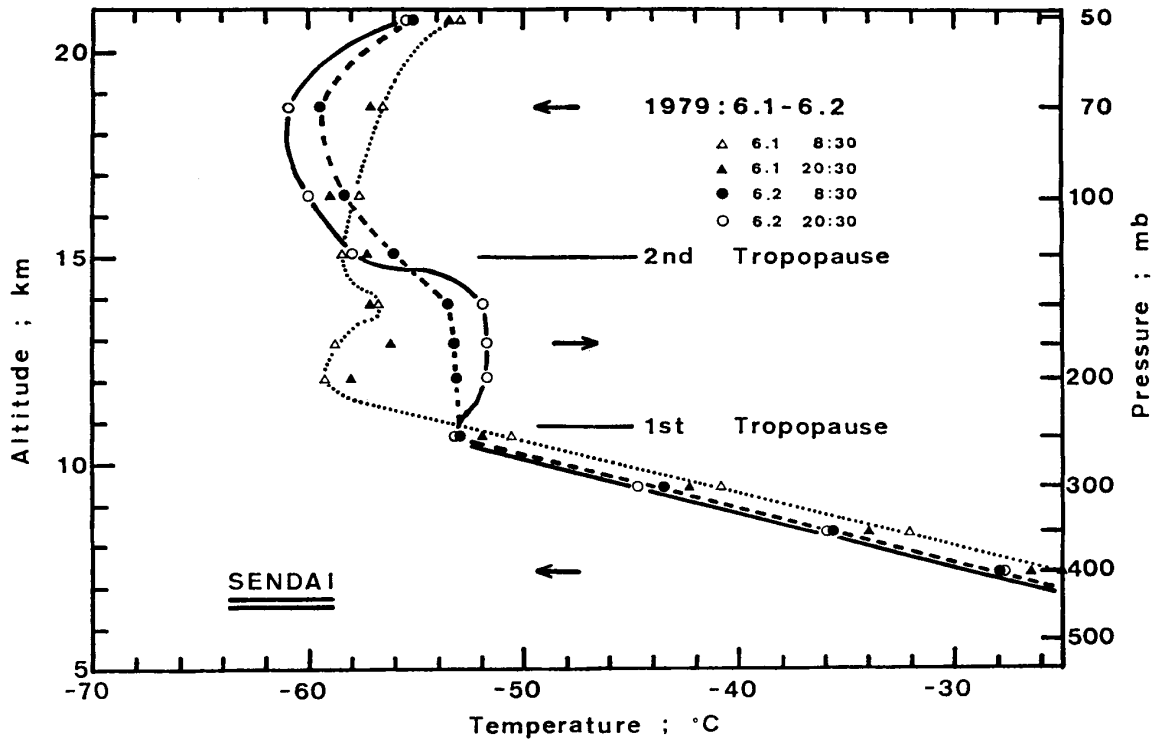

FIG. 4–8. Altitude profile of the atmospheric temperature at Sendai during 6/1–6/2, 1979.

Finally, in relation to our result, a very interesting datum obtained by Kuhn et al. (1969) are presented in Fig. 4–9. The graph shows the drastic change of the stratospheric water vapor density when the observational aircraft passed over the U.S. from the northern California to the central United States.

This figure shows a sudden decrease in the stratospheric water vapor amount. This is because the aircraft has removed from the air mass of the tropical origin to that of the arctic origin. Evidently as the air temperature becomes low, the stratospheric water vapor amount is gradually decreasing as well. Furthermore, it should be noted that the slight increase of 1–2 ppm in the stratospheric water vapor amount takes place in conjunction with the crossing of the weak front. Thus it can be seen that the water vapor concentration in the lower stratosphere is exceedingly subject to the changes in the air temperature and/or the air mass and the large-scale meteorological phenomena such as the crossing of the font in the troposphere.

From the above discussions, the height range at least below 15 km is considerated to have been affected by such a certain meteorological process. However, we cannot judge whether the height range that the actual observation was carried out has been affected or not, though in general the vertical mixing, in this height region is very weak (see, for instance, Matsuno, 1979). If the measured values are contaminated by the extraneous water vapor, for example, the water vapor from the surface of balloon and/or scientific gondola or the inlet system, such an effect should be found for the respective heights. In fact, large mixing ratios of ~ 10 ppmV still remain for 18.6 and 20.2 km height, even if we assume the mixing ratio for 19.4 km heights to be 4 ppmV of Mastenbrook's average value.

From these discussions, we conclude that the high water vapor concentrations obtained in this observation are due to the effects of the actual stratospheric water vapor.

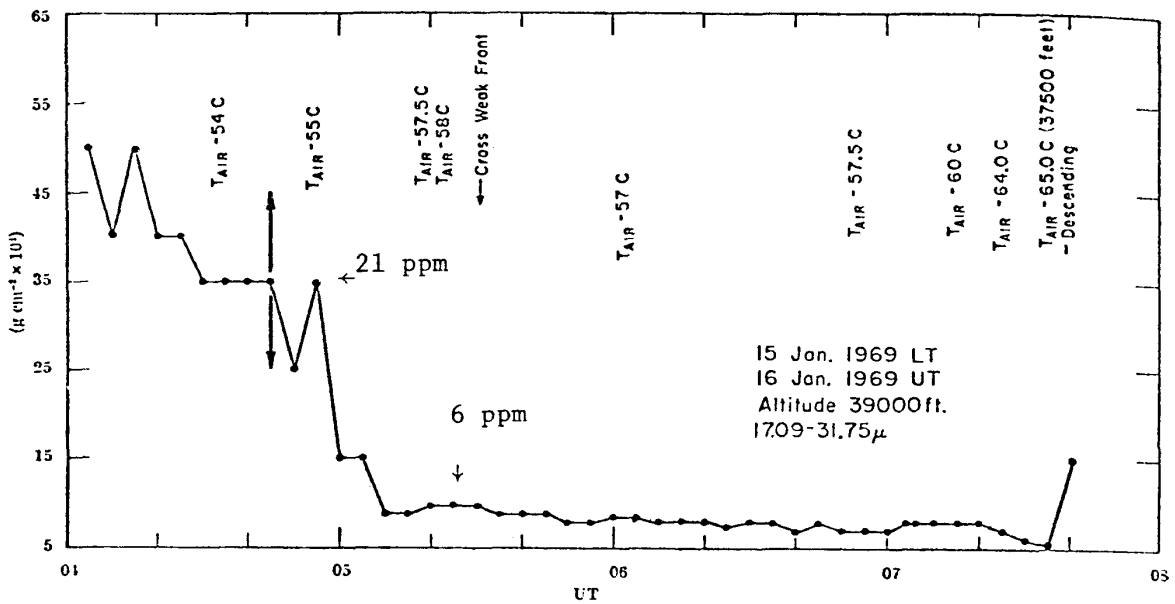

FIG. 4–9. Stratospheric water vapor profile obtained by Kuhn et al. (1969).

4.2 *Contamination from Balloon and Scientific Gondola*

Although the effect of contamination on the measurement can be estimated by the diffusion process, we are now lack of measurement to carry out of such analysis. Therefore, only a brief estimation will be shown here.

The balloon is regarded as a point source of water vapor. In this case, if the flux decrease is dominated by a $(1/4\pi r^2)$-rule (r: distance from balloon), the effects of contamination by balloon is negligibly small, because the water vapor flux from the surface of balloon is estimated to be about 8.7×10^{12} molecules$^{-2}\cdot$cm^{-1} according to Dayton (1960).

As for the contamination from scientific gondola, we have no information at the present stage.

From these discussions, it is rather difficult to estimate exactly the the effects of contamination on the measurement. However, as noted earlier, it is generally said that the data taken during balloon descent are reliable empirically, therefore our data is believed to be free from the contamination by balloon.

4.3 *Flow Process from Troposphere into Stratosphere*

The water vapor content in the stratosphere concerning the flow process from the troposphere into the stratosphere is discussed here. The natural sources of water vapor have already described in Chapter I.

We have already seen from the work of Kuhn et al. (1969) that the water vapor concentration in the lower stratosphere is greatly affected by the changes in the air mass and/or air temperature and the large-scale meteorological phenomena such as the crossing of the front which is recognized in the troposphere. It seems to be quite certain from the previous discussions that a flow of the moist air mass took place before our observation. The water vapor has to be transported upward by moist air flown from the troposphere into the lower stratosphere. Of course, transport by the local eddy diffusion is not effective, because in the altitude region of interest its characteristic time is of the order of several hundreds days (Gudiksen et al., 1968; Matsuno, 1979). Therefore transport of air must be done by a kind of dynamical action probably associated with the turbulences or waves. It has been well established that the exchange of air through tropopause breaks or foldings takes place associated with the cyclone (Briggs and Roach, 1963; Danielsen, 1968). However, little is known about the details of the flow process from troposphere to stratosphere. To clarify its mechanism is of great importance with a view to understanding the coupling between stratosphere and troposphere. It is highly desirable to clarify the process for the exchanges between the stratospheric and tropospheric air.

By the reason described above, measurement of the water vapor density in the troposphere and stratosphere is quite important to solve the above-described problem.

§ 5. Suggestions for Further Experimental Works

In this Section, we discuss some problems associated with the present observa-

tion, and suggest further experimental works.

5.1 *Selection of Water Vapor Absorption Lines*

As we have seen in the course of this work, the σ-band absorption was used as an absorption band for our present observation. It is quite natural that absorption lines which can be used for the present purpose should be selected by taking account of the following factors: (1) Strong absorption line, (2) No absorption band due to the other atmospheric molecules, (3) Intense light source with small power consumption, and (4) Radiation sensor which is easy to handle. Therefore as we have discussed in Section 5 of Chapter III, if measurement to use more intense absorption lines in the $\phi(1.13\mu)$, $\psi(1.38\mu)$, and $\Omega(1.87\mu)$ band region is available by means of compact balloon-borne-diode-laser, more reliable water vapor observation will be possible.

5.2 *Light Source and Detector*

The light emitting diode used in this experiments has several advantages as a light source as described in Subsection 3.2 of Chapter II. However, as its emission profile is considerably broad (half width of the emission profile is $\simeq 45$ nm), we have to use the narrow band-pass filter to get the narrow beam. It is evident from eq. (5a) of Chapter III that the effective (or mean) absorption cross section in the case of the narrow band-pass filter is larger than that in the case of the broad band-pass filter. Accordingly, the most ideal light source is the monochromatic radiation in the filter absorptiometry. To use the laser is the best way to carry out the present measurement. We will be able to use compact balloon-borne diode laser in a few years.

As for the detector, the photomultiplier cannot be used as a radiation sensor, if certain absorption lines among the ϕ, ψ, and Ω absorption bands are adopted. In this wavelength region, there are many *IR* detectors which are classified into two groups, thermal detectors and quantum detectors. Both thermal and quantum detectors are available for the present purpose. However when we make use of quantum detectors, they must be cooled in most cases. In balloon experiment, although the liq. N_2-cooled or liq. He-cooled detectors are often used, the thermal detectors such as the bolometer and Golay cell can provide the sufficient S/N ratio, when we use the laser as a light source.

5.3 *Further Separation from the Balloon*

When we carry out the water vapor measurement in the stratosphere, we have no information on the effects of contamination from the balloon. As we have already discussed in Section 4 of Chapter IV, the way to avoid the extraneous water vapor from the instrument train is to take the data during balloon descent. Moreover further separation of gondola from the balloon will reduce the contamination. As is often carried out in the water vapor observation in the stratosphere, it is of great interest to compare the descent data with the ascent data. This comparison will give informations on the effects of contamination from the instrument train.

5.4 *Differential Absorption Technique*

In the present method, the data obtained by the observation contain the effects of the Rayleigh and Mie scattering. To avoid these effects, we might be able to use the so-called differential absorption method which has been utilized as, for example, the differential absorption lidar (see, for example, Menzies and Shumate, 1978). In our case, the two different wavelengths around 935 nm, λ_{on} and λ_{off} can be selected as light sources by tuning the wavelength with the monochromator, where λ_{on} is the wavelength wich the strong absorption of water vapor occurs and λ_{off} is the off-tuned wavelength which no absorption occurs in this spectral region. If we measure the ratio of the light intensity at wavelength λ_{on} to that at λ_{off}, we can deduce the water vapor density from the difference between the two light intensities.

The water vapor density obtained by this method are apparently free from the 'extraneous' effects such as the Rayleigh and Mie scattering.

Chapter V. GENERAL CONCLUSION

In this thesis, the water vapor content in the stratosphere has been studied. Water vapor causes a variety of interesting phenomena and plays significant roles in the earth's atmosphere. Therefore it is important to know the water vapor concentration in particular in the stratosphere. For the purposes of the present investigation, some spectroscopic measurements have been done and a newly-designed hygrometer which is based on the filter absorptiometry has been developed.

First, high resolution absorption spectra of water vapor were recorded in the 0.94 μm spectral region. From these spectra, the most desirable absorption lines for water vapor measurement were determined.

Absorption cross sections for these absorption lines have been measured based on two different methods in order to evaluate the feasibility of water vapor observation in the stratosphere. One method which is based on the filter absorptiometry gives a value of 1.64×10^{-21} cm$^2\cdot$molecule^{-1} at the line center of 942.836 nm absorption line. On the other hand, a value of 1.73×10^{-21} cm$^2\cdot$molecule^{-1} for the same absorption line has been deduced from another method whose measurements are based on the Lambert-Beer's law. In this case, the maximum errors of these values are less than 10 percent. Therefore, above two methods are available even for any other atmospheric molecules and quite useful and effective for the determination of absorption cross section in the visible to the near infrared spectral region.

We also have developed a new instrument for the water vapor observation in the stratosphere. The present instrument has been designed on the basis of the filter absorptiometry using the multiple-traversal absorption cell with a 9.8 m-long absorption path. Our method has several advantages that is; (1) in situ observation, (2) very simple principle, (3) no assumption and no complicated procedure are necessary, and (4) measurement is available in nighttime as well as in daytime.

Based on this, the water vapor observation in the lower stratosphere has been

carried out at S.B.C. (39°N, 142°E), Japan. To avoid the contamination from balloon, the descent data were taken. The results obtained are approximately 22, 10 and 24 ppm by volume at an altitude of 18.6, 19.4, and 20.2 km respectively. These values correspond to the relative humidity of 15, 5, and 9% respectively.

Aerological data which was taken over Sendai city during the same period showed that the relative humidity below the first tropopause around 11 km was a few times as moist as that of 12 hours before. And the temperature below the first tropopause and above second tropopause (around 15 km) decreased uniformly with time, while in the intermediate region between the first tropopause and second tropopause, the temperature was drastically increasing by some 8°C within 36 hours. From these facts, it is suggested that exchange of air took place through dynamical actions associated with a certain kind of turbulences. This process might account for the high water vapor concentrations which have been measured in the present observation. The mechanism of this process is, however, still unknown at our present stage of knowledge. To understand this mechanism will be useful to discuss the coupling between troposphere and stratosphere. This problem is of great importance not only for the water vapor in the stratosphere itself but also for the terrestrial atmosphere system in general.

Department of Space Science,
Institute of Space and Aeronautical Science,
University of Tokyo
October 20, 1029

References

Ackerman, H., Stratospheric water vapor from high resolution infrared spectra, Planet. Space Sci., **22**, 1265–1267, 1974.

Armstrong, B. H., Spectrum line profiles: The Voigt function, J. Quant. Spectrosc. Radiat. Transfer, **7**, 61–68, 1967.

Barclay, F. R., M. J. W. Elliott, P. Goldsmith, and J. V. Jelley, A direct measurement of the humidity in the stratosphere using a cooled-vapor trap, Quart. J. Roy. Meteorol. Soc., **86**, 259–264, 1960.

Bates, D. R. and M. Nicolet, The photochemistry of atmospheric water vapor, J. Geophys. Res., **55**, 301–327, 1950.

Baumann, W. and R. Mecke, Das rotationsschwingungsspektrum des wasserdampfes. II., Zs. f. Phys., **81**, 445–464, 1933.

Benedict, W. S. and L. D. Kaplan, Calculation of line widths in H_2O-N_2 collisions, J. Chem. Phys., **30**, 388–399, 1959.

Bertaux, J-L. and A. Delannoy, Vertical distribution of H_2O in the stratosphere as determined by UV fluorescence in-situ measurements, Geophys. Res. Lett., **5**, 1017–1020, 1978.

Brewer, A. W., Evidence for a world circulation provided by the measurements of helium and water distribution in the stratosphere, Quart. J. Roy. Meteorol. Soc., **70**, 351–363, 1949.

Brewer, A. W., B. Cwilong, and G. M. B. Dobson, Measurement of absolute humidity in extremely dry air, Proc. Phys. Soc., London, **62**, 52–70, 1948.

Brewer, A. W. and K. P. B. Thomson, A radiometer-sonde for observing stratospheric emission due to water vapor in its rotation bands, Quart. J. Roy. Meteorol. Soc., **98**, 187–192, 1972.

Briggs, J. and W. T. Roach, Aircraft observations near jet stream, Quart. J. Roy. Meteorol. Soc., **89**, 225–247, 1963.

Chaloner, C. P., J. R. Drummond, J. T. Houghton, R. F. Jarnot, and H. K. Roscoe, Stratospheric measurements of H_2O and the diurnal change of NO and NO_2, Nature, **258**, 696–697, 1975.

Chleck, D., Measurements of upper atmosphere water vapor made in situ with a new moisture sensor, Geophys. Res. Lett., **6**, 379–381, 1979.

CIAP Monograph 1, The natural Stratosphere of 1974, Rep. No. DOT-TST-75-51, U.S. Department of Transportation, 1975.

CIAP Monograph 3, Propulsion Effluents in the Stratosphere, Rep. No. DOT-TST-75-52, U.S. Department of Transportation, 1975.

Clemesha, B. R. and D. M. Simonich, Stratospheric dust measurements, 1970–1977, J. Geophys. Res., **83**, 2403–2408, 1978.

Craig, R. A., *The upper atmosphere, Meteorology and Physics*, Academic Press, 1965.

Crutzen, P. J., The impact of the chlorocarbon industry on the ozone layer, J. Geophys. Res., **83**, 345–363, 1978.

Dalgarno, A., Spectral reflectivity in the earth's atmosphere, III. The scattering of light by atomic system, GCA Report No. 62-28, 1962.

Danielsen, E. F., Stratospheric-tropospheric exchange based on radioactivity, ozone and potential vorticity, J. Atm. Sci., **25**, 502–518, 1968.

Dayton, B. B., 1959 6th Natl. Symp. Vac. Technol. Trans., Pergamon Press, 1960.

De Jonckheere, C. G., A measurement of the mixing ratio of water vapor from 15 to 45 km, Quart, J. Roy. Meteorol. Soc., **101**, 21–223, 1975.

Delbouille, L. and G. Roland, *Photometric atlas of the solar spectrum from* λ *7498 to* λ *12016*, Mém. Soc. Roy. Sci. Liège, Special Volume No. 4, 1963.

Dobson, G. M. B., Origin and distribution of the polyatomic molecules in the atmosphere, Proc. Roy. Soc. London, **236**, 187–192, 1956.

Dobson, G. M. B., A. W. Brewer, and B. M. Cwilong, Meteorology of the lower stratosphere, Pro. Roy. Soc., London, A, **185**, 144–175, 1946.

Donahue, T. M., R. J. Cicerone, S. C. Liu, and W. L. Chameides, Effect of odd hydrogen on ozone depletion by chlorine reactions, Geophys. Res. Lett., **3**, 105–108, 1076.

Ehhalt, D. H., L. E. Heidt, R. H. Lueb, and E. A. Martell, Contaminations of CH_4, CO, CO_2, H_2O and N_2O in the upper stratosphere, J. Atm. Sci., **32**, 163–169, 1975.

Ellsaesser, H. W., Water budget of the stratosphere, Proceedings of the third conference of the Climatic Impact Assessment Program, pp. 273–283, Department of Transportation, Washington, D.C., 1974.

Farmer, C. B., Infrared measurements of stratospheric composition, Can. J. Chem., **52**, 1544–1559, 1974.

Fujiwara, M., T. Itabe, and M. Hirono, Sudden increase of stratospheric aerosol content after the eruption of Fuego volcano; Lidar observations in Fukuoka, Rept. Ionos. Space Res. Japan, **29**, 74–78, 1975.

Gates, D. M., Near infrared atmospheric transmission to solar radiation, J. Opt. Soc. Am., **50**, 1299–1304, 1960.

Goldman, A., D. G. Murcray, F. H. Murcray, W. J. Williams, and J. N. Brooks, Distribution of water vapor in the stratosphere as determined from balloon measurements of atmospheric emission spectra in the 24–39 μm region, Appl. Opt., **12**, 1045–1053, 1973a.

Goody, R. M., *Atmospheric Radiation I. Theoretical basis*, Oxford University Press, 1964.

Gudiksen, P. H., A. W. Fairhall, and R. J. Reed, Roles of mean meridional circulation and eddy diffusion in the transport of trace substances in the lower stratosphere, J. Geophys. Res. **73**, 4461–4473, 1968.

Gutnick, M., How dry is the sky ?, J. Geophys. Res., **66**, 2867–2871, 1961.

Harries, J. E., Measurements of stratospheric water vapor using far-infrared techniques, J. Atm. Sci., **30**, 1691–1698, 1973.

Harries, J. E., Measurements of some H-O-N compounds in the stratospheric from Concorde 002, Nature, **241**, 515–518, 1973.

Harries, J. E., D. G. Moss, and N. R. Swann, H_2O, O_3, N_2O and HNO_3 in the arctic stratosphere, Nature, **250**, 475–476, 1974.

Harries, J. R., The distribution of water vapour in the stratosphere, Rev. Geophys. and Space Phys. **14**, 565–575, 1976.

Harries, J. E., D. G. Moss, N. R. W. Swann, and G. F. Neill, Simultaneous measurements of H_2O, NO_2, and HNO_3 in the daytime stratosphere from 15 to 35 km, Nature, **259**, 300–301, 1976.

Heidt, L. E., NCAR reports: Results from cryogenic sampling balloon flight, preprint, 3, 1978.

Herzberg, G., *Molecular Spectra and Molecular Structure II, Infrared and Roman Spectra of Polyatomic molecule*, D. Van Nostrand, Newyork, 1950.

Hesstvedt, E., Mother-of-pearl clouds in Norway, *Geophysica Norvegica*, **20**, 1–29, 1959.

Hirono, M., M. Fujiwara, O. Uchino, and T. Itabe, Observations of aerosol layers in the upper atmosphere by laser radar, Rept. Ionos. Space Res. Japan, **26**, 237–244, 1972.

Hirono, M., M. Fujiwara, O. Uchino, and T. Itabe, Observations of stratospheric aerosol layers by optical radar, Can. J. Chem., **52**, 1560–1568, 1974.

Hirono, M., M. Fujiwara, C. Nagasawa, O. Uchino, and M. Maeda, Observation of the Middle atmosphere with laser radars, Laser Res., **7**, 3–18, 1979 (in Japanese).

Houghton, J. T. and J. S. Seeley, Spectroscopic observations of the water-vapor content of the stratosphere, Quart. J. Roy. Meteorol. Soc., **86**, 358–370, 1960.

Howard, J. N., The transmission of the atmosphere in the infrared, Proc. Inst. Radio Eng., **47**, 1451–1457, 1959.

Hunt, B. G., Photochemistry of ozone in a moist atmosphere, J. Geophys. Res., **71**, 1398, 1966.

Hunten, D. M. and D. F. Strobel, Production and escape of terrestrial hydrogen, J. Atm. Sci., **31**, 305–317, 1974.

Hyson, P. and C. M. R. Platt, Radiometeric measurements of stratospheric water vapor in the southern Hemisphere, J. Geophys. Res., **79**, 5001–5005, 1974.

Itabe, T., M. Fujiwara, and Hirono, Temporal variation of the stratospheric aerosol layer after the Fuego eruption observed by lidar in Fukuoka, J. Meteorol. Soc. Japan, **55**, 606–612, 1977.

Iwasaka, Y. and K. Isono, Lidar observation of the stratospheric aerosols at two different wavelength, 0.6943 μm and 1.06 μm, J. Atm. Terr. Phys., **39**, 117–120, 1977.

Johnston, H. S. and S. Solomon, Thunderstorms as possible micrometeorological sink for stratospheric water, J. Geophys. Res., **84**, 3155–3158, 1979.

Junge, C. E., C. W. Chagnon, and J. E. Manson, Stratospheric aerosols, J. Meteorol., **18**, 81–108, 1961.

Kida, H., A numerical investigation of the atmospheric general circulation and stratospheric-tropospheric mass exchange: II. Lagrangian motion of the atmosphere, J. Meteorol. Soc. Japan, **55**, 71–88, 1977.

Kondratyev, K. Ya., *Radiation in the atmosphere*, International Geophysics Series, vol. 12, 107–123, Academic Press, 1969.

Kuhn, P. M., M. S. Lojko, and E. W. Petersen, Infrared measurements of variations in stratospheric water vapor, Nature, **223**, 462–464, 1969.

Kuhn, P. M., M. S. Lojko, and E. V. Peterson, Water vapor: Stratospheric injection by thunderstorms, Science, **174**, 1319–1321, 1971.

Kuhn, P. M. and L. P. Steams, Latitudinal profiles of stratospheric water vapor, Geophys. Res. Lett., **2**, 227–230, 1975.

Kuhn, P. M., E. Magaziner, and L. P. Stearns, Stratospheric areal distribution of water vapor burden and the jet stream, Geophys. Res. Lett., **3**, 529–532, 1976.

Kuhn, W. R. and J. London, Infrared radiative cooling in the middle atmosphere (30–110 km), J. Atm. Sci., **26**, 189–204, 1969.

Liu, S. C. and T. M. Donahue, Mesospheric hydrogen related to exospheric escape mechanism, J. Atm. Sci., **31**, 2238–2242, 1974.

Liu, S. C., T. M. Donahue, R. J. Cicerone, and W. L. Chameides, Effect of Water Vapor on the destruction of ozone in the stratosphere perturbed by Cl_x or NO_x pollutants, J.

Geophys. Res., **81**, 3111–3118, 1976.
Manabe, S. and R. T. Wetherald, Thermal equilibrium of the atmosphere with a given distribution of relative humidity, J. Atm. Sci., **24**, 241–259, 1967.
Mastenbrook, H. J. and J. E. Dinger, Distribution of water vapor in the stratosphere, J. Geophys. Res., **66**, 1437–1444, 1961.
Mastenbrook, H. J., Water distribution in the stratosphere and high troposphere, J. Atm. Sci., **25**, 299–311, 1968.
Mastenbrook, H. J., The variability of water vapour in the stratosphere, J. Atm. Sci., **28**, 1495–1501, 1971.
Mastenbrook, H. J., Water vapour measurements in the lower stratosphere, Can. J. Chem., **52**, 1527–1531, 1974.
Matsuno, T., Meteorology of the stratosphere, Kagaku (Science), **47**, 2–10, 1977 (in Japanese).
Matsuno, T., Global scale transport process, in *Science of atmospheric environment (ed. G. Yamamoto)*, vol. 2, 192–210, Univ. of Tokyo Press, 1979 (in Japanese).
Matsuno, T., Lagrangian motion of air parcels in the stratosphere in the presence of planetary waves, Pure Appl. Geophys., to be published, 1979.
Matsuno, T., private communication, 1979.
McElroy, M. B. and J. C. McConnell, Nitrous oxide: A natural source of stratospheric NO, J. Atm. Sci., **28**, 1095–1098, 1971.
Mckinnon, D. and H. W. Morewood, Water vapour distribution in the lower stratosphere over north and south America, J. Atm. Sci., **27**, 483–493, 1970.
Menzies, R. T. and M. S. Shumate, Tropospheric ozone distributions measured with an airborne laser absorption spectrometer, J. Geophys. Res., **83**, 4039–4043, 1978.
Molina, M. J. and F. S. Rowland, Stratospheric sink for chlorofluoromethanes: Chlorine atom-catalysed destruction of ozone, Nature, **249**, 810–812, 1974.
Murcray, D. G., F. H. Murcray, W. J. Williams, and F. E. Leslie, Water vapor distribution above 90,000 feet, J. Geophys. Res., **65**, 3641–3649, 1960.
Murcray, D. G., T. G. Kyle, and W. J. Williamson, Distribution of water vapor in the stratosphere as derived from setting sun absorption data, J. Geophys. Res., **74**, 5369–5373, 1969.
Nagata T. and T. Tohmatsu, *Modern Aeronomy*, Syōkabō, Tokyo, 1973 (in Japanese).
Nicolet, M., Ozone and hydrogen reactions, Ann. Géophys., **26**, 531–546, 1970.
Nicolet, M., Aeronomic chemistry of the stratosphere, Planet. Space Sci., **20**, 1671–1702, 1972.
Ogawa, T., Height distribution of minor constituents in the stratosphere, Tenki, **22**, 215–226, 1975 (in Japanese).
Ogawa, T., Chemistry of stratospheric chlorine, J. Meteorol. Soc. Japan, **54**, 294–307, 1976.
Ogawa, T., private communication, 1979.
Patel, C. K. N., E. G. Burkhardt, and C. A. Lambert, Spectroscopic measurements of stratospheric NO and H_2O, Science, **184**, 1173–1176, 1974.
Penner, S. S., *Quantitative Molecular Spectroscopy and Gas Emissivities*, Addison-Wesley Co., Inc., Roading, Mass, 1959.
Pick, D. R. and J. T. Houghton, Measurements of atmospheric infrared emission with a balloon-borne multifilter radiometer, Quart. J. Roy. Meteorol. Soc., **95**, 535–543, 1969.
Pinnick, R. G., J. M. Rosen, and D. J. Hofmann, Stratospheric aerosol measurements III: Optical model calculations, J. Atm. Sci., **33**, 304–314, 1976.
Shimazaki, T. and T. Ogawa, A theoretical model of minor constituents distribution in the stratosphere including diurnal variations, J. Geophys. Res., **79**, 3411–3423, 1974.
Shimazaki, T., *Stratospheric ozone*, Univ. of Tokyo Press, 1979 (in Japanese).
Shindoh, R. and H. Baba, Shin-Jikken-Kagaku-Koza, Kiso-Gijyutsu, 3 Hikari [I], Maruzen Co., 1976 (in Japanese).
Siebert, M., Atmospheric tides, *Advances in Geophysics*, **7**, 105–187, 1961.
Sissenwine, N., D. D. Grantham, and H. A. Salmela, Mid-latitude humidity to 32 km, J. Atm. Sci., **25**, 1129–1140, 1968.
Stanford, J. L., Possible sink for stratospheric water vapor at the winter antarctic pole, J. Atm. Sci., **30**, 1431–1436, 1973.

Stanford, J. L., Stratospheric water vapor upper limits inferred from upper-air observations: Part I. northern hemisphere, Bull. Am. Meteorol. Soc., **55**, 194–212, 1974.

Stolarski, R. S. and R. G. Cicerone, Stratospheric chlorine: A possible sink for ozone, Can. J. Chem., **52**, 1610–1615, 1974.

Streete, J. L., J. H. Taylor, and S. L. Ball, Near IR atmospheric absorption over a 25 km horizontal path at sea level, Appl. Opt. **6**, 489–496, 1967.

Strong, J. and G. N. Plass, The effect of pressure broadening of spectral lines on atmospheric temperature, Astrophys. J., **112**, 365–379, 1950.

Takahashi, F. and K. Hirao, Absorption spectra of water vapor in the near infrared region, ISAS Research Note, RN-72, 1979a.

Takahashi, F., K. Hirao, and T. Itoh, Measurements of absorption cross sections of water vapor in the 0.94 μm region, Bull. Inst. Space Aeronaut. Sci., **15**(B), 97–106, 1979b (in Japanese).

Terui, G., A. Ikushima, and H. Kanai, Digital boxcar integrator and digital lock-in amplifier, Kotai-Butsuri, **8**, 654–662, 1973 (in Japanese).

Uchida, T. and S. Minami, Light detection and Data Processing (4) Lock-In Amplifier and Boxcar Integrator, Bunkō Kenkyū, **23**, 196–207, 1974 (in Japanese).

Van de Hulst, H. C. and J. J. M. Reesinck, Line breadths and Voigt profiles, Astrophys. J., **106**, 121–127, 1947.

Watanabe, T. and T. Tohmatsu, An observational evidence for the seasonal variation of ozone concentration in the upper stratosphere and the mesosphere, Rep. Ionos. Space Res. Japan, **30**, 47–50, 1976.

Weickmann, H. K. and C. C. Van Valin, The sources and sinks of water vapor in the stratosphere, NOAA Tech. Rep. ERL 307- APCL32, U.S. Department of Commerce, 1974.

Weickmann, H. K. and C. C. Van Valin, The sources and sinks of water vapor in the upper atmosphere, paper presented at the international conference on aerospace and aeronautical meteorology, Washington, D.C., May, 1972.

Whiting, E. E., An empirical approximation to the Voigt profiles, J. Quant. Spectrosc. Radiat. Transfer, **8**, 1379–1384, 1968.

Williamson, E. J. and J. T. Houghton, Radiometric measurements of emission from stratospheric water vapor, Quart. J. Roy. Meteorol. Soc., **91**, 330–338, 1966.

Wofsy, S. C., J. C. McConnell, and M. B. McElroy, Atmospheric CH_4, CO, and CO_2, J. Geophys. Res., **77**, 4477–4493, 1972.

Wofsy, S. C. and M. B. McElroy, HO_x, NO_x, and ClO_x; Their role in atmospheric photochemistry, Can. J. Chem., **52**, 1582–1591, 1974.